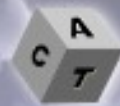




Journal of Advanced Concrete Technology
Materials, Structures and Environment



Stray current-induced development of cement-based microstructure in water-submerged, $\text{Ca}(\text{OH})_2$ -submerged and sealed conditions

Agus Susanto , Dessi A. Koleva , Klaas van Breugel , Kees van Beek


Journal of Advanced Concrete Technology, volume 15 (2017), pp. 244-268

Related Papers [Click to Download full PDF!](#)

Mechanical, electrical and microstructural properties of cement-based materials in conditions of stray current flow

Agus Susanto , Dessi A. Koleva, C[i n\Ub Copuroglu, Kees van Beekž?`UUgj Ub'6fYi [Y`

Journal of Advanced Concrete Technology, volume11 (2013), pp. 119-134



Click to Submit your Papers

Japan Concrete Institute <http://www.j-act.org>



Scientific paper

Stray Current-Induced Development of Cement-Based Microstructure in Water-Submerged, $\text{Ca}(\text{OH})_2$ -Submerged and Sealed Conditions

Agus Susanto^{1*}, Dessi A. Koleva², Klaas van Breugel³ and Kees van Beek⁴

Received 22 November 2016, accepted 7 May 2017

doi:10.3151/jact.15.244

Abstract

This work reports on the development of microstructural and mechanical properties of mortar cubes under the synergistic action of stray current and various environmental/curing conditions. The study refers to specimens cured for 24h only, followed by a 112 days period of partial or full submersion in water or alkaline medium. Additionally, equally prepared mortar specimens were tested in sealed conditions. The outcomes for submerged and saturated conditions were compared to sealed conditions. Three current density regimes were employed i.e. 1 A/m^2 , 100 mA/m^2 , and 10 mA/m^2 , simulating different levels of stray (DC) current environment. The highest level of 1 A/m^2 was also comparable to stray current densities, as measured in field conditions. The tests were designed in a way, so that the effects of diffusion-controlled transport (ions leaching due to concentration gradients), were distinguished from migration-controlled ones (ion/water transport in stray current conditions). Mechanical, microstructural and electrical properties were monitored throughout the test. For water-conditioned specimens, the stray current was found to accelerate degradation processes. This was reflected by decreased compressive strength, reduced electrical resistivity and increased porosity of the matrix. The results were attributed to leaching-out of alkali ions due to concentration gradients, where except diffusion, migration took place i.e. the leaching-out effect was accelerated by water and ions migration in conditions of stray current flow. In contrast, stray current flowing through mortar in sealed conditions (as well as through mortar in alkaline medium) resulted in increased compressive strength and electrical resistivity. These were accompanied by densification of the bulk matrix and reduced porosity. It can be concluded that for a cement-based material at early hydration age, both positive and negative effects of stray current flow can be expected. The level and direction of these effects are dependent on the external environment and the current density levels, where stray currents above 100 mA/m^2 and in conditions of concentration gradients with the external medium, would lead to more pronounced negative effects on microstructural and micromechanical performance.

1. Introduction

During their service life, cement-based materials are exposed to various external environments that can have either beneficial or negative effect on the cement-based matrix. Generally, concrete degrades with age in aggressive environment (e.g. acidic, sodium chloride-containing environments, stray current flow, etc.). For instance, main constituents (as Ca-bearing compounds) of the hydrated cement paste in concrete, when exposed to aqueous solutions, may leach out due to concentra-

tion gradient or chemical potential. Leaching occurs from regions with higher concentration to regions with lower concentration of the diffusing substance (a process occurring for example in underground storage tanks, dams, water tanks and radioactive waste disposal containers). Since calcium leaching coarsens the pore structure, the result is a porous bulk matrix (Jain *et al.* 2009; Puertas *et al.* 2010; Marinoni *et al.* 2008; Gaitero *et al.* 2008; Cheng *et al.* 2012), increased permeability, reduced mechanical strength (Gawin *et al.* 2009; Kamali *et al.* 2003; Marchand *et al.* 2000; Carde *et al.* 1996). Generally, the leaching process starts with a total dissolution of portlandite (calcium hydroxide, CH), ettringite, followed by a progressive decalcification of the calcium-silicate-hydrate (C-S-H) phase. Long term leaching follows a square root of the leaching duration (Ulm *et al.* 1999; Köhl *et al.* 2004). Other degradation processes may occur when aggressive chemical species from the external environment as chlorides, carbon dioxide, sulphates penetrate into the cement-based material, e.g. concrete sulphate attack, corrosion of the steel reinforcement, etc.

When the above chemical and physico-chemical degradation mechanisms are enhanced due to faster ion and water transport, i.e. due to ion migration as for example in conditions of stray current flow, an increased level of

¹PhD student, Faculty of Civil Engineering and Geosciences, Materials and Environment, Delft University of Technology, Delft, The Netherlands.

*Corresponding author, E-mail: a.susanto@tudelft.nl

²Assistant Professor, Faculty of Civil Engineering and Geosciences, Materials and Environment, Delft University of Technology, Delft, The Netherlands.

³Professor, Faculty of Civil Engineering and Geosciences, Materials and Environment, Delft University of Technology, Delft, The Netherlands.

⁴Senior electronics design engineer, The Electronic and Mechanical Support Division (DEMO), Delft University of Technology, Delft, The Netherlands.

structural degradation would be expected. Stray currents were reported to affect not only embedded in concrete steel reinforcement (Bertolini *et al.* 2007; Chen *et al.* 2012; Lingvay *et al.* 2011; Yang *et al.* 2008; Chen *et al.* 2011), but can also induce degradation of the cement-based matrix (Susanto *et al.* 2013). Any electrical field, including stray current, will influence cement hydration by altering ion and water transport. Consequently, stray currents will modify material properties and can affect the behaviour and integrity of a reinforced concrete structure. Negative effects have been reported, e.g. altered bulk matrix properties, reduced mechanical properties, increased permeability (Koleva *et al.* 2008; Susanto *et al.* 2013). Positive effects of electrical current are also reported, but only at early cement hydration age, linked to strength development within “electrical” curing (Bredenkamp *et al.* 1993; CUR-Bouw&Infra 2009).

Several works reported on quantifying the influence of stray current on cement-based materials via modelling approaches only (Wang *et al.* 2010; Xia *et al.* 2013; Peelen *et al.* 2011). In contrast, our previous work combined both experimental and numerical approach, resulting in more insight into the related phenomena. Previously reported was the positive effect of stray current on partially submerged in water mortar specimens at early stages only (<14 days of cement hydration). The positive effect was due to accelerated cement hydration, accompanied by increasing compressive strength, denser pore structure and higher electrical resistivity for the “under current regime”, compared to control specimens. However, a reversed trend was observed at later stages (>28 days), where the stray current induced negative effects, leading to coarsening of the mortar bulk matrix, reduced mechanical and electrical properties. The effect of stray current on cement-based microstructure was *hypothesized* to depend and vary with respect to the environmental conditions and the current density level.

Therefore, the extensive investigation subject to this work, including varying external medium, different curing regimes and higher current densities, was performed in order to elucidate the effect of stray current on cement-based materials. In particular, this work aims to clarify some of the previously posed research questions on different environmental conditions and leaching phenomena. The aim is to clearly distinguish the effects of ions leaching due to concentration gradient from those, resulting from enhanced ion and water migration, i.e. when stray current is involved. Hence, hereby presented and discussed is the effect of stray current flow on mortar specimens submerged in water, compared to stray current effects on mortar in sealed conditions and in conditions of partial or full submersion in alkaline medium ($\text{Ca}(\text{OH})_2$ solution). Except the effect of concentration gradient, an important aspect is the level of stray current density.

In this work, three levels of stray current densities

were applied, considering main points as follows: the lowest current density level of 10 mA/m^2 was employed as a simulation of current flow due to electrochemical protection techniques (e.g. impressed current cathodic protection). Although much lower levels of stray current densities e.g. in the range of 1 to 1.5 mA/m^2 were reported (Charalambous *et al.* 2014; Aylott *et al.* 2013), considering previous studies (Susanto 2013) an increase with a factor of 10 was chosen for obtaining better distinguishable results. The highest level of employed current density of 1 A/m^2 was chosen as comparable to levels also measured in real field situations, i.e. between 1 and 1.5 A/m^2 (Galsgaard and Nielsen 2006). The step in-between i.e. 100 mA/m^2 adds to the series of tested steps by a factor of 10 and for completeness of the tests.

To this end, the aim of this work was to achieve a step forward towards defining the effect of stray current in view of positive or negative influence on cementitious materials’ properties, considering various environmental conditions and practical aspects. The levels of stray currents in real practice are hard to measure, if, in fact, considered at all with respect to concrete material properties. While stray current effects on corrosion of steel reinforcement are largely reported, these effects on concrete bulk properties are normally not of concern. For instance, in practical cases the electrical current flow through reinforced concrete structures from train tracks is about 0.06 Ampere (or 3 A/m^2 if normalised to a cross section area of 180 cm^2 as used in this study). This is three times higher compared to the maximum stray current level applied in this study (i.e. 1 A/m^2 or 0.018 A). Estimation of the resultant corrosion damage over a certain period of time can be performed using Faraday’s law, if the magnitude of stray current is known. For example, metal loss due to corrosion damage from stray current flow with level 0.05A and 1A are about 455 and 9100 g/year, respectively (Riskin 2008). Such calculations cannot be easily made and are not reported for damage quantification with regard to cement-based materials. More importantly, the cumulative effect of stray current on a bulk concrete matrix is perhaps of larger significance, considering the fundamental principles and behaviour of a cement-based matrix with age and with respect to environmental conditions. This includes the effect of electrical currents (incl. stray current) on cement hydration, potential leaching-out effects, microstructural and micromechanical properties. This is also where the present work aims to contribute to the present state-of-the-art on the subject.

2. Experimental materials and methods

2.1 Materials

Mortar cubes of $40 \text{ mm} \times 40 \text{ mm} \times 40 \text{ mm}$ were cast, using OPC CEM I 42.5N with water-to-cement ratio of 0.5 and cement-to-sand ratio of 1:3. The chemical composition (in weight (%)) of CEM I 42.5N (ENCI, NL) is as follows: 63.9% CaO; 20.6% SiO_2 ; 5.01% Al_2O_3 ;

Table 1 Test matrix: □ - compressive strength; ○ - MIP/ESEM tests; Δ - el. resistivity (* Full details on this (marked) investigation are reported in (Susanto *et al.* 2013).

Current density Groups	Hydration age	Condition and environment				
		Partly submerged		Fully submerged		Sealed
		H ₂ O	Ca(OH) ₂	H ₂ O	Ca(OH) ₂	
Control	3	Δ *	-	Δ	-	□ ○ Δ
	7	Δ *	-	-	-	□ Δ
	14	□ Δ *	□ Δ	□ Δ	□ Δ	-
	28	□ ○ Δ *	□ ○ Δ	□ ○ Δ	□ ○ Δ	□ ○ Δ
	84	□ Δ *	□ Δ	□	□ Δ	-
	112	□ ○ Δ *	□ ○ Δ	□ ○ Δ	□ ○ Δ	□ Δ
10mA/m ²	3	Δ *	-	-	-	-
	7	Δ *	-	-	-	-
	14	□ Δ *	□ Δ	-	-	-
	28	□ ○ Δ *	□ ○ Δ	-	-	-
	84	□ Δ *	□ Δ	-	-	-
	112	□ ○ Δ *	□ ○ Δ	-	-	-
100mA/m ²	3	-	-	Δ	-	□ ○ Δ
	7	-	-	-	-	□ Δ
	14	-	-	□ Δ	□ Δ	-
	28	-	-	□ ○ Δ	□ ○ Δ	□ ○ Δ
	84	-	-	□	□ Δ	-
	112	-	-	□ ○ Δ	□ ○ Δ	□ Δ
1A/m ²	3	-	-	□ Δ	-	□ ○ Δ
	7	-	-	-	-	□ Δ
	14	-	-	□ Δ	□ Δ	-
	28	-	-	□ ○ Δ	□ ○ Δ	□ ○ Δ
	84	-	-	□	□ Δ	-
	112	-	-	□ ○ Δ	□ ○ Δ	□ Δ

3.25% Fe₂O₃; 2.68% SO₃; 0.65% K₂O; 0.3% Na₂O. After casting and prior to conditioning, the specimens were cured in a fog-room of 98% RH, 20°C for 24 hours. For partly submerged and fully submerged conditions: the specimens were treated in water or 0.02M Ca(OH)₂ solution (Seidell *et al.* 1953). For sealed conditions: a specifically designed mould was used, where the specimens were sealed with a rubber gel sealant 24h after casting and remained insulated from each other in the mould (Fig. 1).

2.2 Sample designation and current regimes

Table 1 summarizes the experimental conditions and studied specimen-groups. Four groups of experiments were conducted in different conditions (submerged, partly submerged, sealed condition), varying environment (water, 0.02M Ca(OH)₂) and three levels of DC current density (10 mA/m², 100 mA/m², 1A/m²). The current regimes were adjusted through external current sources, following previously reported set-up for partly submerged conditions (Susanto *et al.* 2013), Fig. 1d) and a specifically designed one for sealed conditions, Fig. 1a,c). The electrical current flow was “injected” via surface area A, in m², Fig. 1c,d), calculated based on the geometrical orientation of the specimens and set-up - 0.27 m x 0.04 m for submerged conditions (Fig. 1d) and 0.04 m x 0.04 m for sealed condition (Fig. 1c). Figure 1(a, b, c) presents the experimental set up for sealed conditions, where the electrical current was applied per cube, via cast-in conductive plates (brass mesh), completely covering the cross-sections A of the cubes (Fig.

1c). Fig. 1c) also depicts the sampling strategy for MIP and ESEM analysis and the geometrical location for microstructural analysis: middle section for fully or partly submerged conditions and middle section and sides for sealed conditions. More details with regard to Fig. 1c) are discussed in the relevant results section for sealed conditions. To be noted is that for both MIP and ESEM microstructural analysis, the comparison of results refers to identically handled specimens and identical geometrical location within one test series.

Multiplexer devices (PC connected) were used to automatically output the electrical resistance of the mortar specimens in real time (the current supply was interrupted in the time of the measurement, details in section 2.3.2 below). The electrical current was applied from 24h of hydration age onwards i.e. immediately after demoulding of the specimens for submerged conditions and after sealing the moulds for the sealed conditions. The tests duration was 112 days.

2.3 Methods

2.3.1 Standard compressive strength

Standard compressive strength tests were performed on 40×40×40 mm mortar cubes at the hydration ages of 3(7), 14, 28(84) and 112 days. Three replicate mortar specimens were taken out from the conditioning set-up, cloth-dried and tested within a 30 min time interval.

2.3.2 Mortar electrical resistivity

The development of electrical properties of the mortar cubes in both control and “under current” conditions

was measured by recording electrical resistivity as output from PC-controlled multiplexer devices. A “2-pin method” was used, where the “pins” were initially cast-in brass plates with dimensions equal to the sides of the mortar cubes (Fig. 1). In order to minimise polarisation effects, the resistance was measured by applying an alternating DC current of 1mA at a frequency of 1 kHz. A PC-controlled R-meter was used, the output being the resistance value, calculated based on measured voltage at the time of current interruption. For the “under current” regime (groups 10 mA/m², 100 mA/m² and 1A/m²), the resistance measurement was performed after current supply interruption of approx. 30 min and surface drying of the cubes. The electrical resistivity was calculated using Ohm’s Law: $\rho=R.A/l$, where ρ is the resistivity in Ohm.m, R is the resistance in Ohm, A is the cross-section of the mortar cube in m², and l is the length in m.

2.3.3 Determination of pore structure parameters

Porosity and pore size distribution of all specimens in all tested conditions were evaluated by Mercury Intrusion Porosimetry (MIP) and through Environmental scanning electron microscopy (ESEM). The experimental procedures for both MIP and ESEM followed already reported sequence of sample preparation, where cement hydration was ceased by submersion in liquid nitrogen, followed by freeze-drying until reaching a constant

weight (Ye 2003; Sumanasooriya *et al.* 2009; Struble *et al.* 1989; Kjellsen *et al.* 2003; Ye *et al.* 2002). The samples for both MIP and ESEM analysis were taken from identical geometrical location in the cubes for each test series (Fig. 1c). The MIP tests were carried out by using Micromeritics Poresizer 9320 (with a maximum pressure of 207 MPa). The drawbacks of MIP, e.g. “ink-bottle effect”, surface tension and contact angle within Hg intrusion/extrusion, etc. are well known and reported in numerous works (e.g. Diamond *et al.* 1995; Winslow *et al.* 1970; Willis *et al.* 1998). However, MIP is largely employed to study the bulk matrix of cement-based materials, including mortar and concrete (Ye 2003; Laskar *et al.* 1997; Kumara *et al.* 2004). Therefore, by “bulk matrix” in this study, the total volume of the mortar matrix refers to MIP, while the bulk cement paste only was evaluated by ESEM image analysis. More importantly, absolute values are not claimed, but rather a comparative analysis between equally handled specimens from identical geometrical location in the same test series is considered, in view of the effect of stray current and relevant environmental conditions. ESEM imaging and image analysis have been successfully used in studying the pore structure of cement-based materials (Lange *et al.* 1994; Diamond *et al.* 1995; Olson *et al.* 1997). The image analysis in this work was performed on an average of 35 locations per sample of 20 × 20 mm size. The image analysis complies with previously reported methodology for pore structure and phase distribution analy-

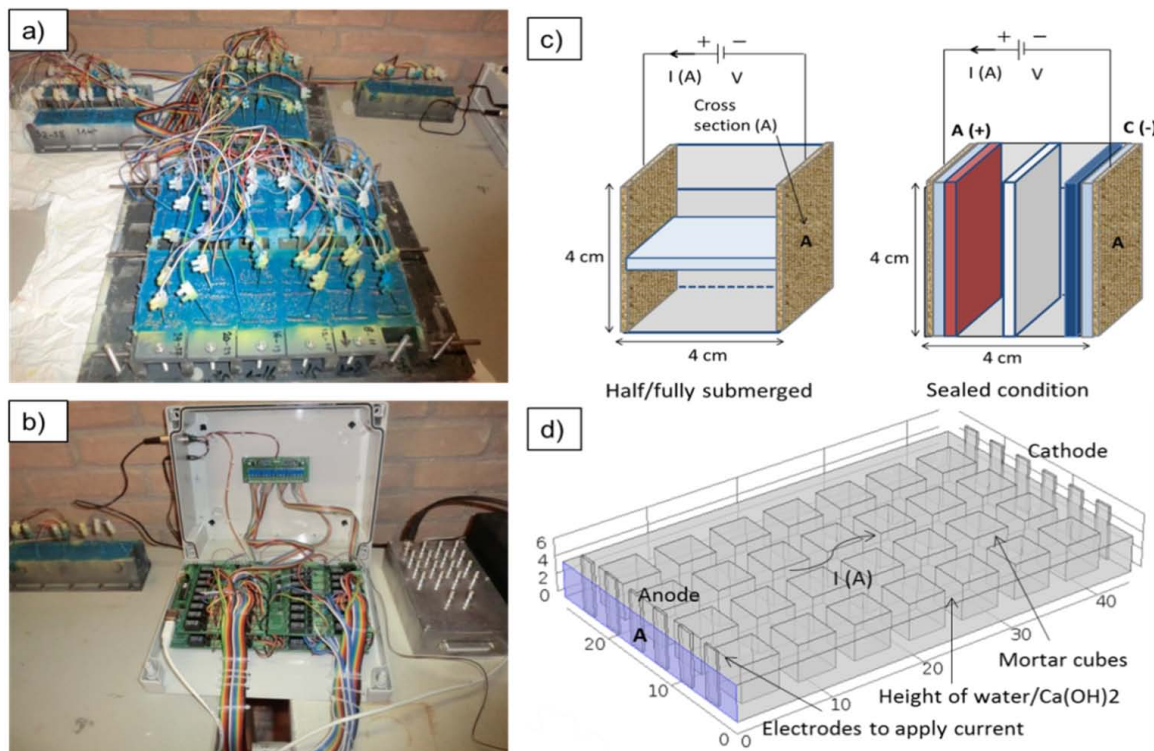


Fig. 1 Experimental set-up, electrical devices, multiplexer to automatically record resistance of the mortar specimens, and schematic presentation of the electrical current application through the cross section (A) of mortar specimens for sealed condition (a, b, c); schematic experimental set up for submerged (partially or full) conditions (d), as also previously reported (Susanto *et al.* 2013).

sis of cement based materials, implementing mathematical morphology and stereology approaches (Serra 1982; Hu *et al.* 2003). Main details and considerations with regard to image analysis are as follows.

2.3.4 Image analysis

The image analysis complied with the generally used methodology for pore structure analysis of cement based materials (Ye 2003; Hu 2004). The image analysis performed in this study is as reported in (Koleva 2007), main considerations of which are as follows: Scanning electron microscopy (using ESEM Philips XL30) was employed for visualization and microstructure investigations. Section images of the specimens were obtained with backscattered electron (BSE) mode (a set of ESEM images were made at random locations throughout the full size of polished sections). The physical size of the reference region of each image is 226 μm in length and 154 μm in width, with the resolution of 0.317 $\mu\text{m}/\text{pixel}$ (corresponding to a magnification of 500x). Small capillary pores play an important role in the transport properties of cement based specimens (Hu 2003). Hence, it is necessary to strike a balance between a representative area element revealing sufficiently large pore section, and a satisfactory resolution for detection of these small capillary pores. Higher magnification could be expected to reveal more details in the pore structure, however, as reported in (Hu 2003), resolutions of 0.293 $\mu\text{m}/\text{pixel}$ (1000x) and 0.146 $\mu\text{m}/\text{pixel}$ (2000x) gave similar values. The image analysis was performed using OPTIMAS software package. The combination of ESEM images and quantitative image analysis allows deriving structural information of the pore space, such as the porosity and critical pore size. On the basis of mathematical morphology transformations, a pore size distribution can be obtained by using a sequence of similarly shaped structuring elements of increasing size (Serra 1982). In this study, the so called ‘opening distribution’ was used, where the binary image is opened by a series of squares of increasing size (Hu 2003; Koleva 2007). The original BSE image (or a selected area, excluding any aggregate particles, if any) is segmented by applying a grey-level threshold to create a binary image, reflecting the pore phase. The threshold grey level between porosity and solid phases is selected based on the shape of the histogram of the BSE image. The anhydrous material and calcium hydroxide (CH) have fairly uniform grey levels, resulting in certain peaks in the histograms. Due to variation in composition, the grey levels of the other hydration products (calcium silica-hydrate (C-S-H)) form a shallower but still identifiable peak in the histograms. For properly choosing a threshold value of the grey level for segmentation of the pore space, it has been found that consistent results can be obtained by selecting an arbitrary point on the lower slope of the peak produced by the other hydration products (Scrivener 2004). The binary image is then subjected to quantitative image analysis for derivation of structural pa-

rameters (pore size distribution, critical pore size, etc.). As aforementioned, the ‘opening distribution’ technique was used, whereby the binary image is opened by a series of squares of increasing size (Hu 2003). The cumulative pore size distribution curve is obtained by plotting the pore area fraction after an opening operation versus linear dimension of the structuring element. This gives a type of ‘size’ classification in the case of an interconnected structure, like pore space in mortar. The critical pore size can be conceived as the diameter of the pore that completes the first interconnected pore pathway in a network, developed by a procedure of sequentially adding pores of diminishing size to this network.

2.3.5 Chemical analysis

Chemical analysis of the conditioning water (external medium) was performed to determine changes in alkali ions concentration (Na^+ , K^+ and Ca^{++}) due to ions leaching-out from the mortar cubes. The tests were performed using Inductive Coupled Plasma Spectrometry (ICP-AES) after 1, 3, 14, 28, 44, 56 and until 112 days of conditioning of the mortar specimens. Additionally, chemical analysis for hydrated (chemically bound) water at certain hydration ages (1, 7, 14, 28, 84 and 112 days of conditioning) and for some of the tested specimens was determined according NEN 5931 (which is a standard loss of ignition test). According to NEN 5931 standard, the mass loss per gram of original cement was measured between 105°C and 775°C. The specimens were stored in the oven with temperature 105°C to constant weight (at least 12 hours) and transferred to a desiccator to cool down to room temperature. Afterwards, the specimens were conditioned at 775°C for at least 3 hours (but no more than 6 hours). After cooling of the specimens, the mass loss was determined. Based on the bound water content, the degree of hydration was calculated, using the following equation (Copeland *et al.* 1953):

$$\alpha = \left(\frac{W_n}{c} \right) / \left(\frac{W_n}{c} \right)_{\max} \quad (1)$$

where $\left(\frac{W_n}{c} \right)$ is non-evaporable water content per gram

of original cement in the mixture and $\left(\frac{W_n}{c} \right)_{\max}$ is $\left(\frac{W_n}{c} \right)$

for complete hydration.

The non-evaporable water content per gram of original cement in the mixture W_n/c is calculated as follow (Copeland *et al.* 1953):

$$\frac{W_n}{c} = \frac{W_1}{W_2} (1-L) - 1 \quad (2)$$

where W_1 is the mass of paste prior to ignition (g), W_2 is the mass of paste after ignition (g), and L is the loss of ignition for the sample of the original dry cement powder (g/g of original cement).

Table 2 Non-evaporable water content for major phases (individual constituents) of cement.

Cement Phase	Coefficient ($w_{1..w_4}$)	Mineral composition of cement CEM I 42.5 (% by weight)
	(g water/g cement phase) (Neville 1981; Taylor 1990)	
C ₃ S	0.23	0.62
C ₂ S	0.21	0.105
C ₃ A	0.40	0.073
C ₄ AF	0.37	0.102

The $\left(\frac{W_n}{c}\right)$ for complete hydration $\left(\left(\frac{W_n}{c}\right)_{max}\right)$ mainly depends on the clinker composition of the cements and the amount of reacted cement and can be calculated using the following equation (Copeland *et al.* 1960):

$$\left(\frac{W_n}{c}\right)_{max} = w_1 * (C_3S) + w_2 * (C_2S) + w_3 * (C_3A) + w_4 * (C_4AF) \quad (3)$$

where $w_{1..4}$ is non evaporable water content for individual constituents (g/g) and the designations in bracket (..) is the content of major constituents of the cement considered (g).

By using Eq. (3) and the data in Table 2, the value of 0.238 can be obtained for the term $\left(\frac{W_n}{c}\right)_{max}$. This value is close to the previously reported results, e.g. 0.23

(Taylor 1990) or in a range between 0.23 and 0.25 (Sun *et al.* 2005).

3. Results and discussion

3.1 Compressive strength

The compressive strength development of cement-based materials is determined by several factors, including water-to-cement ratio, cement type, admixtures and curing conditions including humidity, temperature and age (Hu 2004; Mehta *et al.* 2001). Generally, compressive strength increases with the progress of cement hydration and is directly related to microstructural development of the cement-based matrix with time (with maturity development). **Figure 2** presents the recorded compressive strength as a function of hydration age for mortar specimens as follows: *partly submerged in water and Ca(OH)₂* (**Fig. 2a**), as a comparison for control specimens and “under current” condition at the lowest current density level of 10 mA/m²; *fully submerged in water* (**Fig. 2b**) and in Ca(OH)₂ (**Fig. 2c**) - control and “under current” conditions at current density levels of 100 mA/m² and 1 A/m² - **Fig. 2b**); *sealed conditions* (**Fig. 2d**) - control and “under current” at current density levels of 100 mA/m² and 1A/m².

The varying environment i.e. water or Ca(OH)₂, as well as the different levels of stray current (10 mA/m², 100 mA/m² and 1 A/m²) were designed to elucidate the

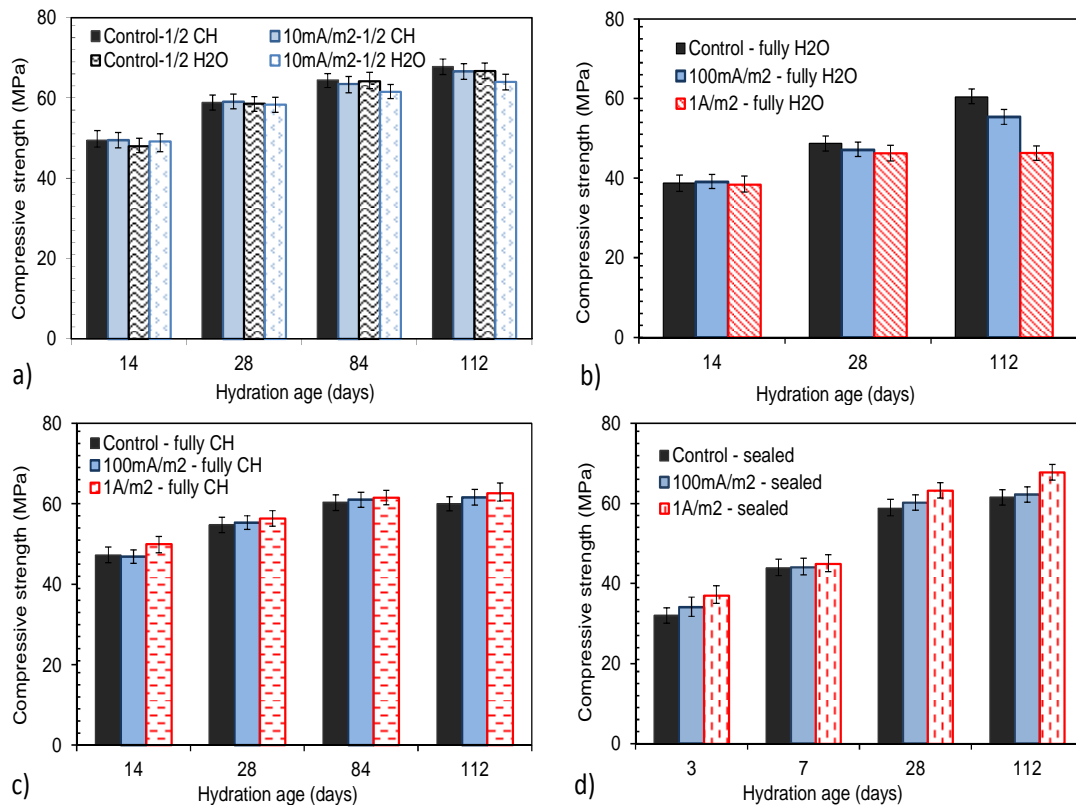


Fig. 2 Compressive strength as a function of hydration age for mortar specimens in rest and “under current” conditions: (a) partly submerged in H₂O and Ca(OH)₂ solution; (b) fully submerged in H₂O; (c) fully submerged in Ca(OH)₂ solution; (d) sealed condition.

effects of ion and water diffusion and ion and water migration, separately or as a synergy. It was expected that leaching-out would occur in water environment, will be minimum in alkaline medium and will not be relevant for sealed conditions. Ion and water migration were a factor when current flow was involved. The resulting mechanical properties were expected to vary with respect to the external medium, the level of stray current density and the above transport mechanisms.

As shown in the **Fig. 2**, the compressive strength for all mortar specimens tends to increase with time of conditioning and with on-going cement hydration. This was as expected, and as observed, for all conditions and irrespective of external medium or current density levels. At 28 days of age all specimen groups present compressive strength in the range of 60-65MPa, with the exception of water-submerged conditions, where approx. 45MPa was recorded. Despite this difference, the recorded compressive strength fulfils the expected from OPC CEM I 42.5N minimum mechanical properties at 28 days of age. The importance of the tests was also in view of recording performance with prolonged treatment, with relevance to environment and current density levels, which are discussed in what follows.

For *partly submerged conditions* in control and “under current” regimes at the lowest current density levels (10 mA/m^2) - **Fig. 2a**, there was no substantial effect of the treatment and/or the current flow on compressive strength development. For mortar specimens partly submerged in Ca(OH)_2 solution, similar compressive strength development was observed for both control and “ 10 mA/m^2 ” groups. However, a general trend to lower compressive strength values towards the end of the test was recorded for the “under current” regime - group 10 mA/m^2 , partly submerged in water.

For *fully submerged conditions* (**Figs. 2b** and **2c**), a more pronounced effect of both external medium and current flow was already observed, bearing in mind that in these conditions the current density level was also higher than that in partly submerged conditions i.e. 100 mA/m^2 and 1 A/m^2 . For water submerged specimens (**Fig. 2b**) the effect of current flow was especially pronounced for the specimens subjected to the highest current density level of 1 A/m^2 , where 45 MPa was recorded after 112 days, while 60 MPa was recorded for the control group at the same age and equal environmental conditions (**Fig. 2b**). A reduction of compressive strength between 28 days of age and the end of the test (112 days) was recorded for the 1 A/m^2 group only. The specimens in group “ 100 mA/m^2 ” maintained higher values at the end of the test (approx. 50MPa), but in a lower range, if compared to control conditions (60MPa). In contrast, the fully submerged in Ca(OH)_2 specimens, **Fig. 2c**, exhibit an increasing trend only of compressive strength development over time, irrespective of the current regime. As seen from **Fig. 2c**, a slight increase even of compressive strength was recorded for mortar in the “under current” regimes. This effect was again more

pronounced for the “ 1 A/m^2 ” group if compared to the lower current density level of 100 mA/m^2 and control specimens.

For *sealed conditions* - **Fig. 2d**, an increase only of compressive strength was relevant for all tested specimens. A more significant effect was again relevant to the highest current density regime (1 A/m^2), in which the mortar specimens exhibited the highest compressive strength at the end of the test ($\sim 65 \text{ MPa}$), (**Fig. 2d**).

What can be concluded from the results in this section is as follows: the development of compressive strength is related to cement hydration with time (with age). This follows the increase in maturity of the cement-based bulk matrix. Consequently, in control (rest) conditions, when other factors were not relevant, the compressive strength would present an increasing trend, followed by stabilisation. The evolution of mechanical properties, following microstructural development, however, is directly linked to the chemical reactions within the cement hydration process. Cement hydration on the other hand is a process, involving (among other factors) ion and water transport due to diffusion and/or migration (capillary suction and permeation were not of significance in the conditions of this work, and are therefore not discussed). In conditions of current flow, diffusion and migration are taking place in parallel. Therefore, enhanced ion and water transport, as in “under current” conditions, would result in altered (mostly enhanced at early stage) cement hydration. Enhanced ion and water transport will also lead to elevated alkali ions leaching-out in conditions, where concentration gradients between the mortar matrix and the external medium are present. Consequently, competing or parallel mechanisms would be relevant for the “under current” regimes: on one hand, enhanced cement hydration, microstructure densification and mechanical strength development *at early stage* will be relevant for all tested specimens. These will dominate throughout the test, i.e. including also the later stages of the test for sealed and Ca(OH)_2 -conditioned specimens.

Enhanced alkali ions leaching and potentially reversed effects on microstructural development, and mechanical performance respectively, *at later stages* will be relevant for water-conditioned specimens. These mechanisms will be affected by the absence or presence of current flow and were expected to be more pronounced for higher current density levels (i.e. enhanced ions and water migration), as actually observed and recorded. In other words, the effect of stray current on mechanical properties is negative, when a concentration gradient between the cement-based material and external environment is present. In contrast, the effect of stray current would be positive at earlier ages of the cement-based system when concentration gradients are minimum or none i.e. when leaching is avoided.

Chemical analysis of the external medium (for water-treated specimens), together with overall microstructural characterisation of the bulk mortar matrix for all tested

conditions, elucidate and support the observed mechanical performance in control and “under current” conditions. The results and discussion on these aspects are presented in the following sections.

3.2 Chemical analysis of the external medium

When a cement-based material is in a prolonged contact with water, dissolution of cement hydrates will occur (due to alkali ions (Ca^{2+} , Na^+ , K^+) leaching). The transport of sodium and potassium is faster than that for calcium ions (Saito *et al.* 1992), and more pronounced at early stages (less mature cement matrix, hence more open pore structure), whereas stable and/or negligible with longer treatment. Leaching of calcium ions promotes coarsening of the pore structure, leads to increased transport properties (permeability, diffusivity) and decrease in mechanical properties (Roessler *et al.* 1985, Young *et al.* 1988). Several studies report on calcium ions leaching from cement-based materials immersed in water (Alonso *et al.* 2006; Faucon *et al.* 1996; Faucon *et al.* 1998; Haga *et al.* 2005; Maltais *et al.* 2004). Calcium leaching was also tested and reported when accelerated methods were applied, involving electrical or chemical gradients (Ryu *et al.* 2002; Saito *et al.* 1992; Wittmann 1997). The results showed that the application of a potential gradient to mortar specimens can be successfully used to assess deterioration mechanisms due to calcium ions leaching.

In this work, the dissolution process, in terms of alkali ions leaching, was only relevant to the partly submerged and fully submerged in water mortar specimens, with applied current density of 10 mA/m², 100 mA/m² and 1 A/m², respectively. Obviously, leaching was not expected for sealed conditions and in $\text{Ca}(\text{OH})_2$ environment. In the former case, there was no aqueous external environment. In the latter case, calcium leaching was expected to be minimum or none, since there was no concentration gradient or chemical potential between the mortar specimens and the external $\text{Ca}(\text{OH})_2$ solution. Therefore, chemical analysis of the external aqueous medium was performed only for the groups of water-treated specimens.

The concentration of leached-out calcium, sodium and potassium (in mg/l) in the external medium was recorded after 1, 3, 14, 28, 44, 56 and 112 days (Fig. 3). The concentration of relevant ions in the external solution was analysed at each of the above stages, after which the medium was exchanged with a fresh one until a subsequent exchange at the next stage. As expected, the leaching process was faster at early ages (early hydration age, higher porosity) and gradually stabilised at later ages, along with increasing the maturity level of the mortar specimens.

As previously reported (Susanto 2013), current density of 10mA/m² in partly submerged in water conditions accelerated the calcium leaching process approx. 1.27 times, if compared to control conditions. Fig. 3a) presents the result for fully submerged in water specimens, subjected to the higher current density level regimes i.e. 100 mA/m² and 1A/m² in comparison to control specimens in these series. The calcium ions concentration in the external medium after 56 days was 567.3 mg/l, 1099.18 mg/l and 1254 mg/l for control cases, 100 mA/m², and 1 A/m², respectively. Calcium leaching increased with 1.93 times for the lower current density regime and 2.04 times for the 1 A/m² regime, if compared to the control specimens. There was no further substantial change in the calcium ions concentration between 56 and 112 days.

As above mentioned, absolute values are not claimed, but only trends of material behaviour are discussed, in relation to the effects of stray current for all test series. It can be concluded that irrespective of the current density level (100 mA/m² or 1A/m²), calcium leaching was enhanced for the “under current” regimes, if compared to the control cases (Fig. 3a). Leaching of sodium (Na^+) and potassium (K^+) ions was also recorded (Figs. 3b)c). Na^+ and K^+ ions have higher solubility and mobility in the pore solution than that of Ca^{2+} ions. As a consequence, Na^+ and K^+ ions will dominate the diffusion and/or migration process more significantly in the beginning of the tests, and will not vary substantially on later stages, as also reported by Babaahmadi *et al.* (Babaahmadi *et al.* 2015). As can be observed in Figs.

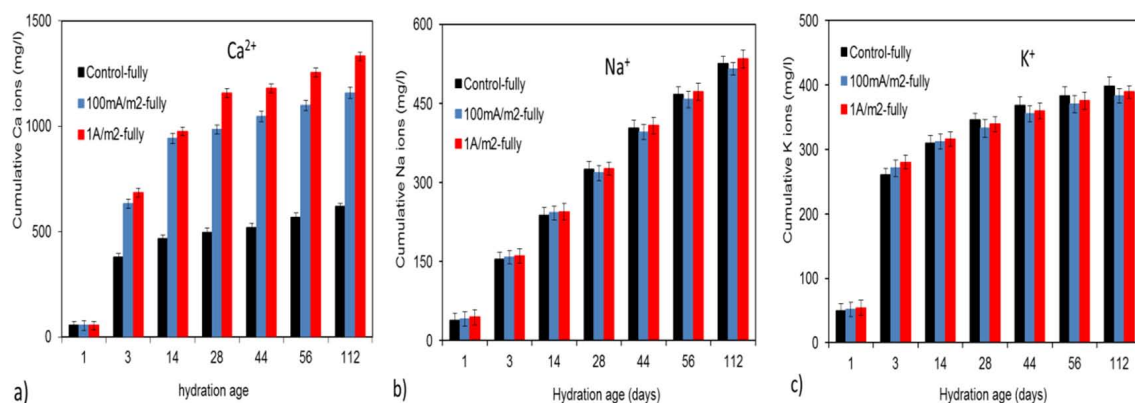


Fig. 3 Cumulative concentration of calcium (a), sodium (b) and potassium (c) in the external medium due to leaching-out of mortar specimens, fully submerged in water (comparison of control (no current) and “under current” regimes).

3b)c), leaching out of sodium and potassium was relevant and gradually increased over time for all specimens and conditions. The concentration of leached out Na^+ and K^+ ions for the “under current” specimens was not significantly different from that for the control specimens on later ages. This is in accordance with the abovementioned mechanisms and outcomes from other studies and related to the increasing portion of disconnected pore network with age of the mortar matrix, which is independent from the dissolution of calcium bearing phases and re-distribution of the pore network e.g. enlargement of initially smaller pores. Overall, for the “under current” conditions the current flowing through both immersed mortar matrix will logically accelerate ion and water transport and consequently promote the leaching process. This effect has to be judged also from the view point of microstructure development with time of conditioning. The consequence of calcium ions leaching in particular is an increase of porosity and a global decrease in mechanical performance (compressive strength) of cement-based materials (Carde *et al.* 1996; Nehdi *et al.* 2011; Saito *et al.* 1992; Saito *et al.* 1999). Therefore, the leaching process will be determined not only by the ion and water migration within the connected pore network, but would be largely dependent on microstructural alteration over time. Hence, the leaching-out effects, or limitations thereof, could be counterbalanced as well, resulting in similar amounts of leached out alkali ions for otherwise different conditions. For the hereby tested series of specimens, and as can be observed in **Fig. 3**, higher current density promoted higher leaching-out effects.

3.3 Microstructural analysis – MIP results

Figure 4 to **Fig. 7** depict MIP-derived porosity and pore size distribution for the bulk matrix of all tested specimens. The plots present an overlay of results for 28 days of age and the latest tested age of 112 days (3 days and 84 days of age for some groups are also presented). The discussion is in view of trends for pore network development in time and in varying experimental conditions,

rather than comparing absolute values. **Figure 4** shows the MIP results as an overlay of two replicates for mortar specimens submerged in water solution at 28 days. It can be seen from **Fig 4** that MIP data have a good reproducibility.

3.3.1 The effect of external medium

Partly submerged conditions, H_2O and alkaline ($\text{Ca}(\text{OH})_2$) external medium: **Fig. 5** presents the MIP results for control specimens and those subjected to 10 mA/m^2 current flow in partly submerged conditions. The MIP results show that for water-conditioned control specimens, a reduction in porosity was observed between 28 days and 84 days but increase towards 112 days of age, **Fig. 5a)b)**. Similarly, first reduction and later-on increase in porosity holds for the “under current”, water-conditioned specimens (**Fig. 5a**), however, in these conditions a more pronounced re-distribution of pore size was observed in the course of the experiment between 28 and 112 days of age (**Fig. 5b**). Both porosity and pore size maintained higher values for the “under current” (10 mA/m^2) regime, compared to control conditions i.e. 9.6% higher at 28 days of age, 10.3 % at 84 days of age and 6.9% at 112 days of age. In contrast, for $\text{Ca}(\text{OH})_2$ -conditioned mortar, stray current at the same level of 10 mA/m^2 induced densification at 28 days of age and no substantial changes at 112 days, **Fig. 5c)d)**. The control specimens in this series also presented reduction in porosity and pore size between 28 days and 112 days.

Concentration gradients were not relevant for the $\text{Ca}(\text{OH})_2$ -conditioned specimens, hence densification only (reduced porosity) was observed due to ongoing cement hydration. For “under current”, water-conditioned specimens, diffusion controlled transport was in parallel (or counter-acting) with migration-controlled transport (along with cement hydration). Therefore, a more pronounced coarsening of the matrix and changes in pore size distribution was observed. In other words, migration enhanced the leaching-out process, resulting in pore size re-distribution i.e. enlarging

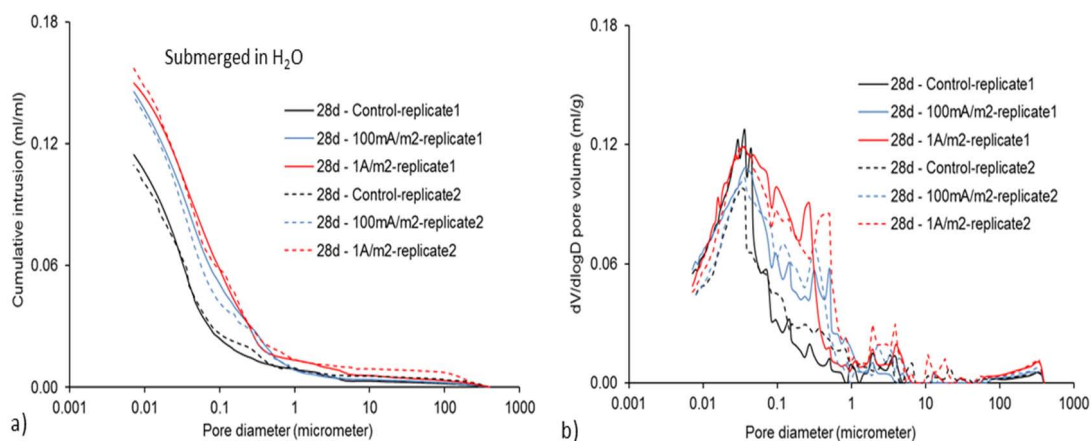


Fig. 4 Example overlay of porosity (a) and pore size distribution (b) obtained from replicates of MIP data for mortar specimens submerged in water solution at 28 days of conditioning time.

pores of initially smaller size. For the Ca(OH)_2 -conditioned specimens, migration did not have a significant effect, although a slight re-distribution of the pore network (in the range of pore size larger than $0.317 \mu\text{m}$) was observed in the MIP results (marked regions in Fig. 5c,d) and confirmed by ESEM image analysis (discussed further below in Section 3.4).

Fully submerged conditions (H_2O and alkaline (Ca(OH)_2) external medium) and Sealed conditions: Figures 6 and 7 present the MIP results for specimens in fully submerged and sealed conditions, respectively. For *water-conditioned specimens*, the mechanisms controlling pore structure development were: a) cement hydration and b) diffusion-controlled water and ion transport under concentration gradient – for control cases, together with c) migration-controlled ion and water transport – for “under current” cases. For *Ca(OH)_2 -conditioned and sealed specimens*, two mechanisms were predominant: a) cement hydration and c) migration-controlled transport. The effect of cement hydration for all groups would be seen in densification of the bulk matrix with time in both control and “under current” regimes. The changes under a synergetic effect of stray current and varying external medium are discussed in what follows.

3.3.2 The effect of stray current and varying medium

Control specimens in all conditions: Figs. 6a, b) show the water conditioned group, where the effect of hydration alone was minimal, with almost no change in porosity between 28 and 112 days. Figs. 6c,d) and Fig. 7a,b) depict the Ca(OH)_2 condition and sealed specimens, respectively, where the effect of cement hydration alone is well pronounced, with well visible reduction in porosity from earlier ages to 112 days. For the water conditioned control specimens, the effect of cement hydration would be counterbalanced by leaching-out and subsequent re-distribution of initially smaller pores towards larger size, evident from Fig. 6b (marked regions). For the control specimens in Ca(OH)_2 and sealed, concentration gradient is not present and leaching-out not relevant.

“Under current” conditions: For specimens in water, the concentration gradient (diffusion-controlled transport) adds-up to the migration-controlled transport. As can be seen in Fig. 6a), the higher the current density level, the higher the level of observed structural modification. For 28 days of age, higher porosity was recorded for specimens in the 100mA and 1A groups, compared to controls. Porosity increased for the “under current” regime at 28 days of age with ca. 31.8% and 26.78% for current density levels 1A/m^2 and at 100mA/m^2 , respec-

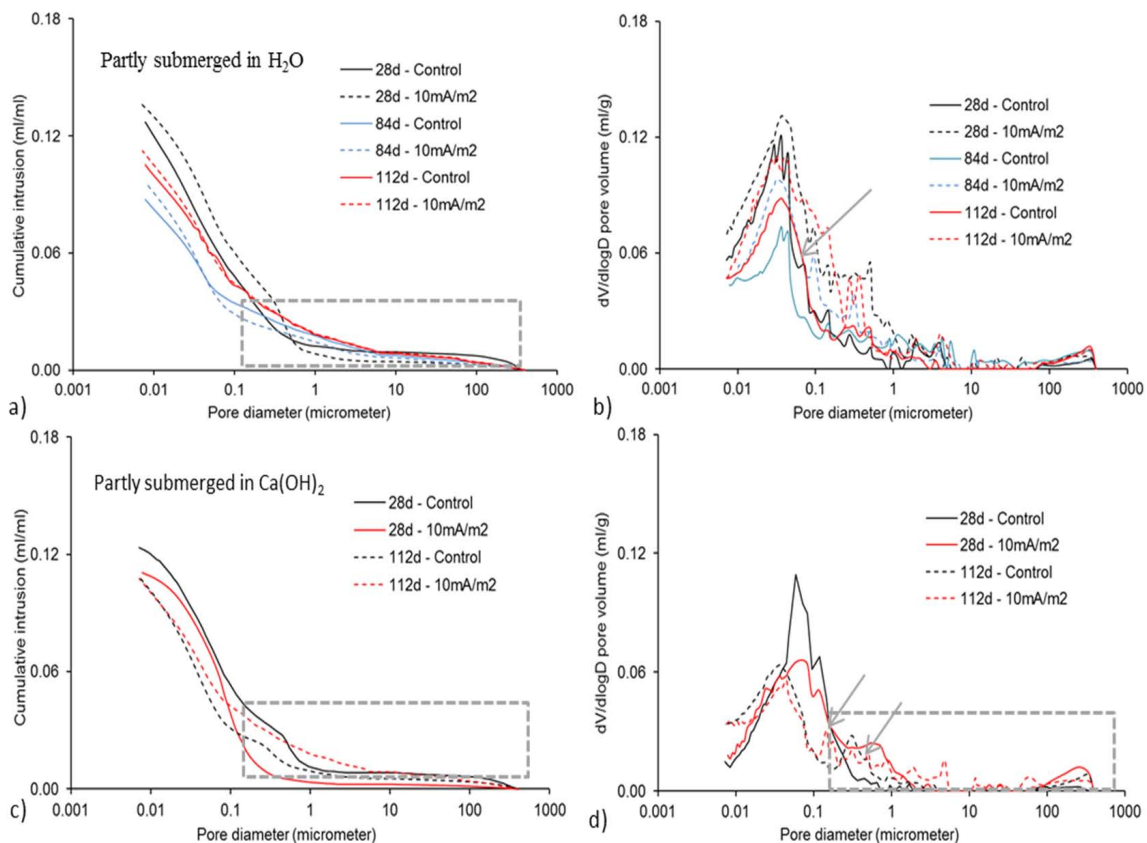


Fig. 5 MIP-derived porosity and pore size distribution for mortar at 28 days, 84(112) days of age - control and “under current” conditions, 10 mA/m^2 : (a, b) partly submerged in water; (c, d) partly submerged in Ca(OH)_2 solution.

tively, compared to control specimens. At 112 days of age the increase was with ca. 15.34% and 4.76% for the “under current” specimens. This was accompanied by an obvious re-distribution of pore size for these specimens from (potentially) smaller pore size to pore enlargement, evidenced by the significant distortion of the differential curves between 0.5µm and 1µm at both 28 days and 112 days of age (Fig. 6b, marked region). The effect is similar to the partly submerged in water conditions (Fig. 5a**), but more significant due to the higher current density levels (along with larger relative humidity, as in saturated condition). At the age of 112**

days, the trend of increased porosity and pore size re-distribution for water treated specimens remained. At both 28 and 112 days, the most significant microstructural changes were observed for the highest current density level of 1A/m².

For Ca(OH)₂-treated specimens, the effect of stray current was positive at 28 days of age, if judged from the reduction in porosity for the “under current” specimens – Fig. 6c**d). For these specimens, leaching-out was not relevant (no concentration gradient present). Therefore, enhanced ion and water migration in “under current” conditions resulted in enhanced cement hydra-**

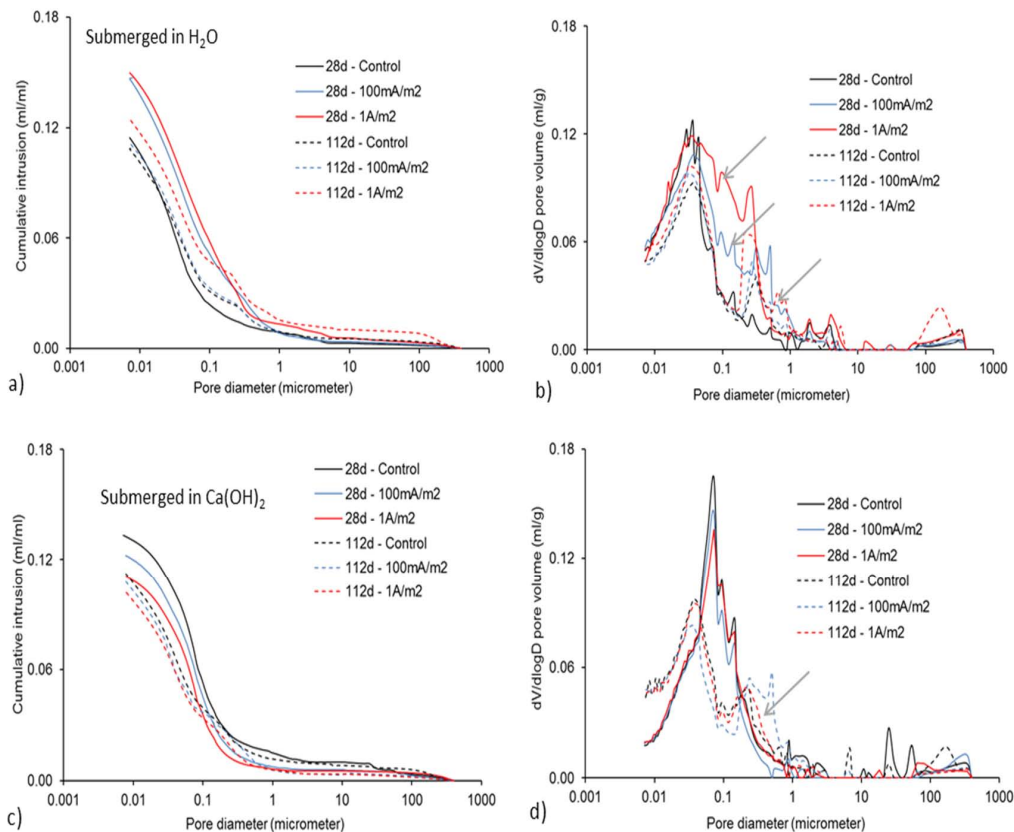


Fig. 6 MIP-derived porosity and pore size distribution for mortar at 28 days and 112 days of age for control and “under current” conditions of **100 mA/m²** and **1 A/m²**: (a, b) fully submerged in water; (c, d) fully submerged in Ca(OH)₂

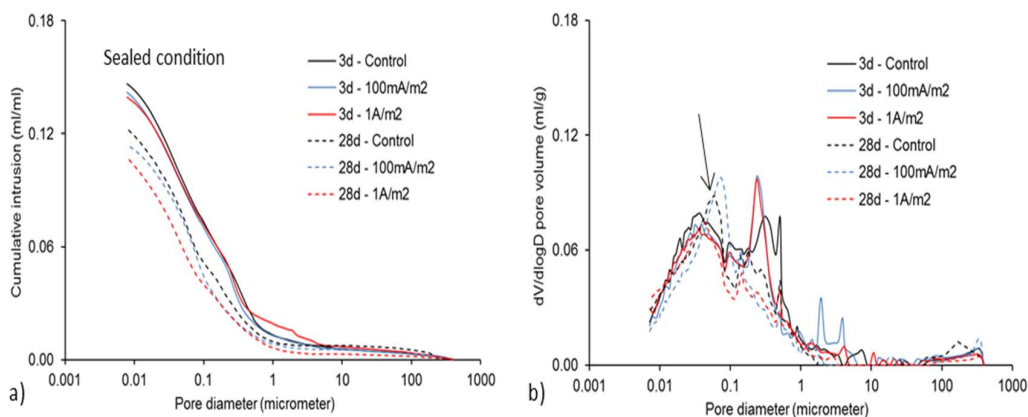


Fig. 7 MIP-derived porosity and pore size distribution for **sealed** mortar at 3 and 28 days of age - control and “under current” of **100 mA/m²** & **1 A/m²**.

tion (Fig. 10), followed by reduction in total porosity at earlier stages (28 days) and no significant difference in porosity at the later stage of 112 days. Critical pore size remained similar and not affected by the current flow at 28 days of age, while re-structuring of the pore network in terms of pore size distribution was observed for 112 days (Fig. 6d). This change is attributed to the effect of current flow and, similarly to the water-conditioned specimens, was more pronounced for the higher level of current density of 1A/m^2 .

Sealed conditions (Fig. 7), the MIP analysis was performed at a very early hydration age – 3 days, and at 28 days. As can be observed (and as expected due to the fresh matrix), porosity and pore size reduced from 3 days to 28 days for all sealed specimens. At the stage of 3 days, no significant change was observed between control and “under current” conditions (Fig. 7a), slightly reduced porosity was recorded in the presence of current flow. After 28 days, a more pronounced effect of the current flow was already observed (Fig. 7a,b), with reduced porosity and pore size, more significant for the specimens at the higher current density level of 1A/m^2 .

If a comparison is made between $\text{Ca}(\text{OH})_2$ -treated specimens and sealed specimens for the stage of 28 days of age, the following can be noted: the difference between control and “under current” regimes (Fig. 7a and Fig. 6c) was comparable for both conditions. Although limited migration-controlled ion and water transport for the sealed specimens would be relevant (transport processes limited to the pore water only), the absence of concentration gradient in both test series determined

similar microstructural development. For both series, the effect of current flow appeared to be only positive for the time frame of the test, with reduced porosity and re-distribution towards smaller pore size over time (Figs. 6c,d; 7a,b). Similarly to all other tested conditions, the effect of the larger current density level of 1A/m^2 was more pronounced, compared to the lower level of 100mA/m^2 .

3.4 Microstructural properties as derived by ESEM image analysis

3.4.1 Partly submerged conditions, H_2O and alkaline ($\text{Ca}(\text{OH})_2$) external medium:

Figures. 8, 9, 11, 12 present the bulk matrix for partly submerged (water and $\text{Ca}(\text{OH})_2$) specimens and the relevant pore structure analysis after 28 days and 84 (112) days of conditioning. Figure 8 depicts the bulk cement paste of water conditioned specimens at 28 days and 84 days of age, Fig. 9 presents the pore structure analysis from 7 days of age, through 28, 56, 84 and 112 days of age. As can be clearly observed in Fig. 9 coarsening of the matrix between 28 days and 112 days of age was relevant for the specimens in water. The effect is more pronounced for the “under current” regimes. An initially positive effect of the stray current was observed, Fig. 9a), reflected by matrix densification in “under current” conditions (compare 7 days result in Fig. 9a) for specimens R (control) and S (10mA/m^2). At this early stage the critical pore size remained similar, which was as expected for a fresh mortar matrix (24h cured only).

At 28 and 56 days of age similar values were recorded for both S and R specimens, slightly higher for

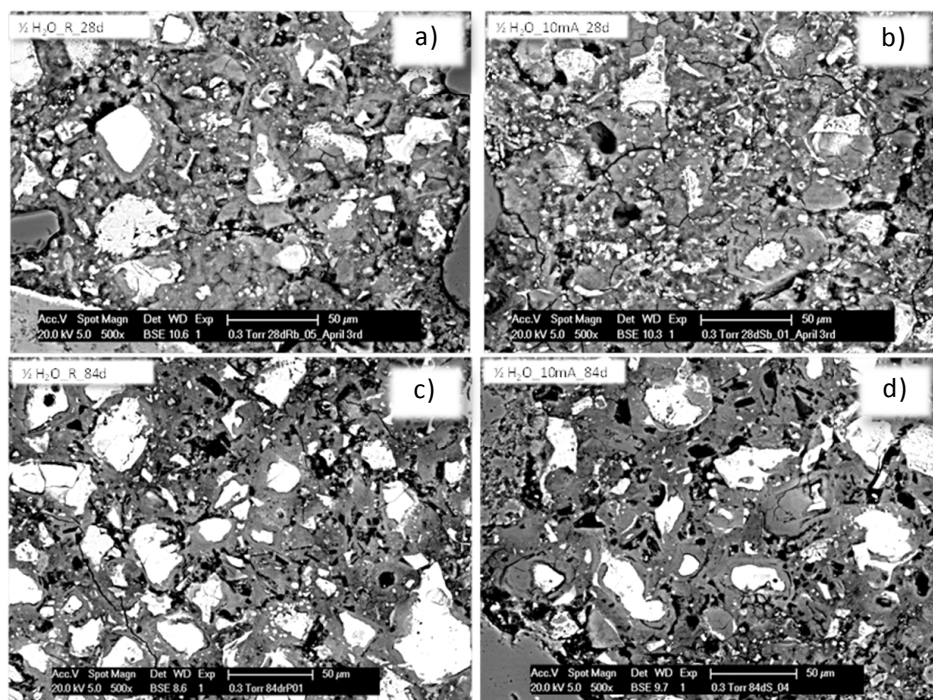


Fig. 8 ESEM micrographs, 500x of mortar bulk matrix at 28 days (top row) and 84 days of age (bottom row) in **partly submerged in water** conditions: control (a, c) and “under current” regime (10mA/m^2) (b, d).

the former case (Fig. 9a, b). Critical pore size remained the same for control conditions, R and decreased for “under current” conditions, S. After 84 days and at the end of the test, coarsening was observed with an already larger difference in pore structure parameters, with increase of porosity and pore size in both R and S conditions, (Fig. 9b). The pore structure alterations would be mainly attributed to leaching-out related coarsening in the sense of enlargement of initially smaller pores. Although a straightforward correlation between MIP and ESEM image analysis cannot be made for several reasons, e.g. the nature of parameters derivation and/or the fact that MIP tests refer to the full volume of material tested, while image analysis refers only to the bulk cement paste, the results from image analysis are in line with those from MIP as far as the effect of stray current is considered and especially with prolonged treatment. Additionally, image analysis is only relevant to pore space larger than 0.317 μm (marked region e.g. in Fig. 5a). To that end, the MIP and image analysis results for the control specimens between 28 days and 84 days of age are contradictory at a first glance, while in line between 84 days and 112 days. The MIP results (Fig. 5a) depict a reduction in overall porosity between 28 and 84 days and increase between 84 and 112 days, while im-

age analysis presents reduction in porosity between 7 and 56 days of age, but increase between 56 and 112 days of age (Fig. 9). The changes in porosity derived by image analysis are accompanied with a larger critical pore size at 28 days (1.92 μm, Fig. 9a), reducing to 0.95 μm at 56 days and increase to 1.3 μm and 1.9 μm at 84 days and 112 days, Fig. 9b). These alterations were not fully detected by MIP, although the differential curves show a large variation for pore sizes, larger than 0.05 μm (marked region in Fig. 5b) at later stages. This outcome is as expected due the fact that mortar was tested (rather than cement paste), resulting in a significant contribution of the matrix heterogeneity within the MIP tests, while the ESEM image analysis is based on direct observations of the bulk cement paste matrix.

Summarising, for partly submerged in water specimens, the alliance of counteracting enhanced ion and water transport (potentially enhanced cement hydration) and (enhanced) leaching-out in conditions of stray-current, resulted in a more pronounced matrix degradation at the end of the test, if compared to control conditions. In fact, the initially enhanced cement hydration due to current flow, was evidenced by the amount of hydrated (chemically bound) water, derived by chemical analysis - Fig. 10a) for water-conditioned specimens.

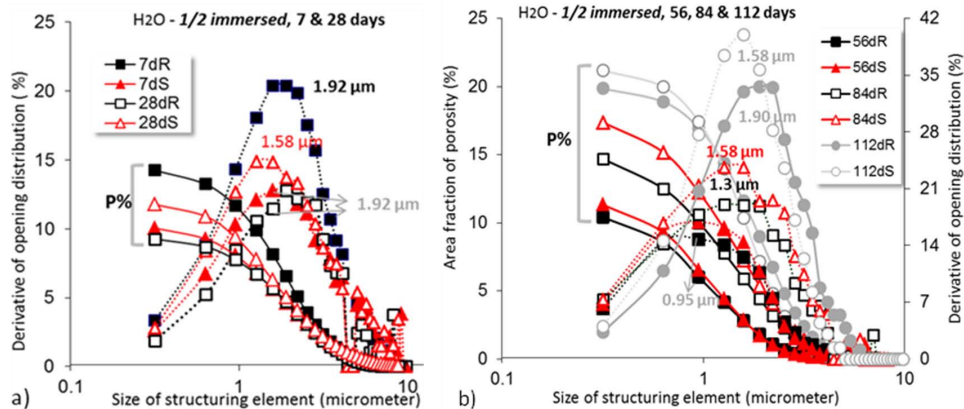


Fig. 9 Porosity and pore size distribution – mortar bulk matrix in **partly submerged in water** conditions in control and “under current” regime (10 mA/m²)– a) overlay of results for 7 and 28 days of age; b) overlay of results for 56, 84 and 112 days of age.

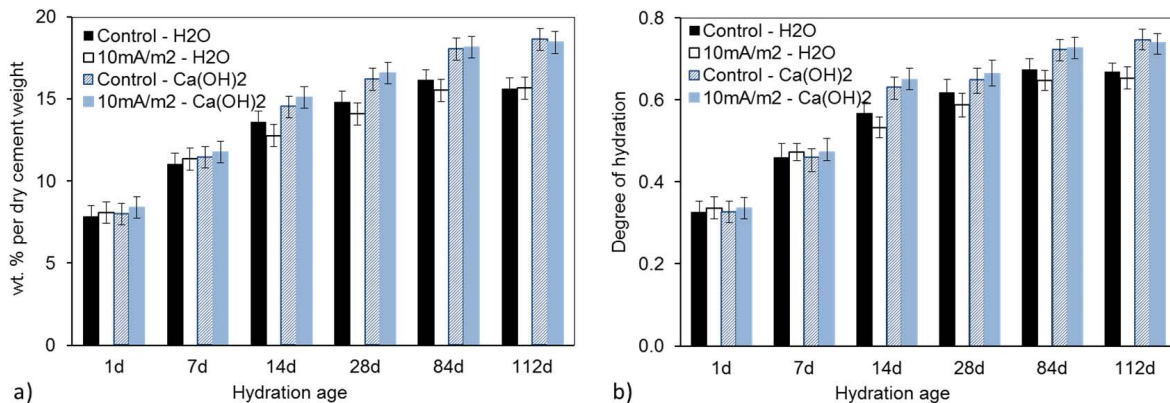


Fig. 10 (a) Weight percent of hydrated (chemically bound water) per dry cement weight for specimens partly-submerged in water and in Ca(OH)₂ at various hydration ages; (b) degree of hydration, calculated as specified in Section 2.3.5.

While the initial stages showed elevated hydrated water content in “under current” specimens, compared to control ones, this trend was reversed after 14 days of age, **Fig. 10a**). The difference is not significant, but clearly supports the fact that with on-going cement hydration, the hydration rate increased over time for all cases, however, was counteracted by leaching-out (**Fig. 3**) due to diffusion and/or migration-controlled ion and water transport. The effect of current flow was initially positive (**Fig. 10a**), but later on (>14 days), negative.

In contrast to the partly-submerged in water specimens (**Figs. 8, 9**), the test series of partly-submerged in Ca(OH)_2 mortar cubes (**Figs. 11, 12**) present a different trend of pore structure development. It is well visible that the microstructural variation between control and

under current conditions at both 28 days and 112 days of age was not as significant (**Fig. 12**), as otherwise clearly observed for the partly-submerged in water specimens (**Fig. 9**). At 28 days of age (**Fig. 12a**), porosity and critical pore size remained in the same range for all regimes, both significantly lower if compared to the partly-submerged in water specimens (**Fig. 9a**). Total porosity decreased from 28 days to 112 days (**Fig. 12a, b**), but maintained higher for the “under current” regime. As can be observed from the differential curves in **Fig. 12b**), although critical pore size remained similar, a slight re-distribution in pore size seemed to be relevant for both control and under current specimens between 28 days and 112 days, which was not as expected. This is in line with the MIP results for this series (**Fig. 5c, d**),

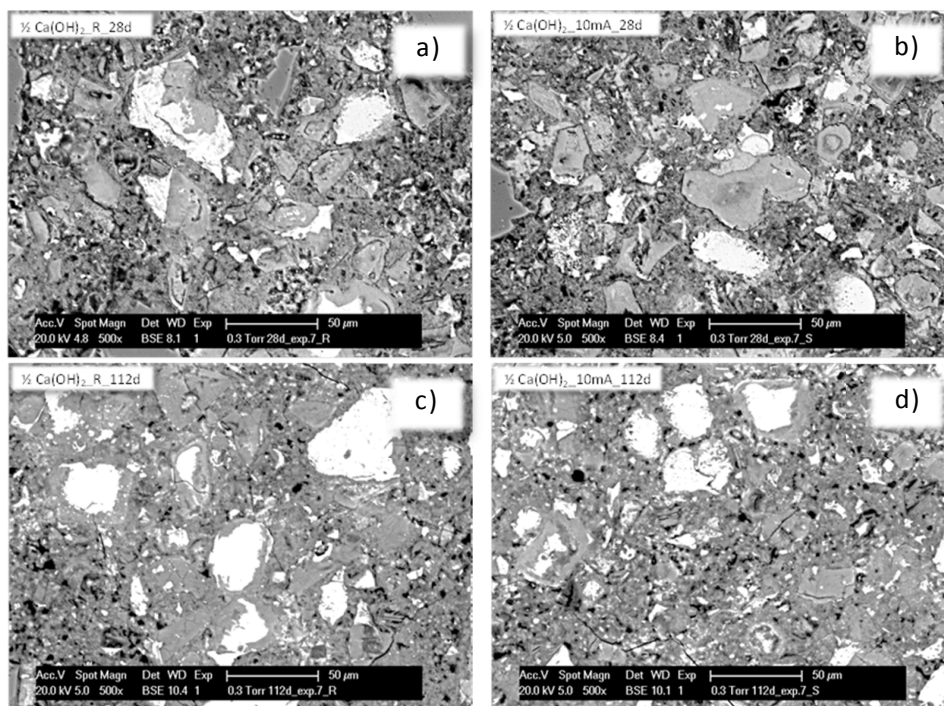


Fig. 11 ESEM micrographs, 500x of mortar bulk matrix at 28 days (top row) and 112 days of age (bottom row) - **partly submerged in Ca(OH)_2** conditions for control (a, c) and “under current” regime (10mA/m²) (b, d).

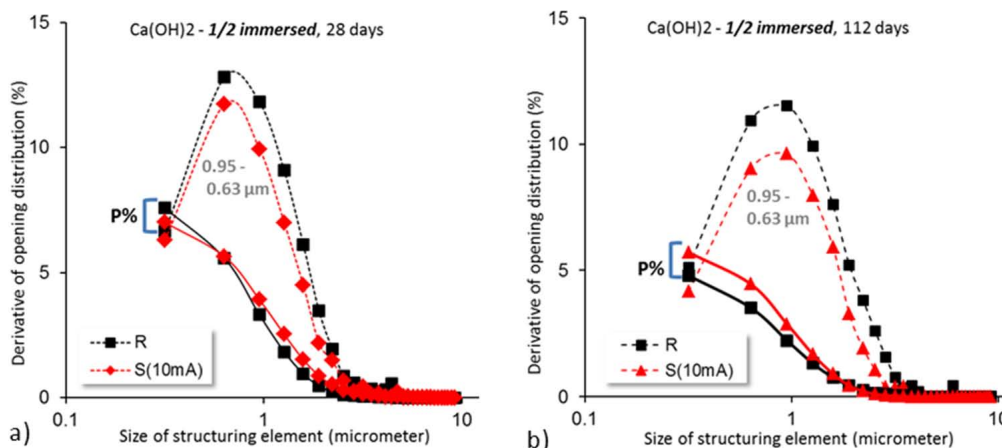


Fig. 12 Porosity and pore size distribution for mortar bulk matrix in control and “under current” regime (10 mA/m²) - **partly submerged in Ca(OH)_2** conditions – a) overlay of results for 28 days of age; b) overlay of results for 112 days of age.

showing re-structuring in the family of capillary pores ($> 0.1 \mu\text{m}$). The result can be interpreted as follows: in partly submerged $\text{Ca}(\text{OH})_2$ conditions, on-going cement hydration would be enhanced when stray current was involved. Therefore, densification of the bulk matrix at earlier stages (28 days) was expected for the “under current” conditions and was as observed (Fig. 12a), although not significant. No concentration gradient was relevant between the submerged portion of the mortar cubes and the external medium. However, concentration gradient was possible between the bottom (submerged) part of the cube and the top (on air) part. Therefore, a slight coarsening of the pore structure in “under current” conditions, compared to control conditions, is possible and was as observed, (Figs. 5d, 12b). This is attributed to uneven relative humidity in the total volume of the specimens.

The above results and discussion for partly-submerged in $\text{Ca}(\text{OH})_2$ specimens were supported by the recorded hydrated water content and the derived degree of hydration, respectively, as depicted in Fig.10a,b). Similarly to the partly-submerged in water conditions, slightly enhanced hydration rate was relevant for the “under current” regime in $\text{Ca}(\text{OH})_2$ medium at earlier ages, with no further significant effects at later stages. Fig. 10 also clearly shows the effect of external medium on hydration rate and cement hydration in general. The difference in values between water-treated and $\text{Ca}(\text{OH})_2$ treated specimens (Fig. 10a,b) is well evident and corresponding to the already discussed microstructural differences and pore network parameters for the two groups.

3.4.2 Fully submerged conditions, H_2O and alkaline ($\text{Ca}(\text{OH})_2$) external medium: Figures 13 to 16 present micrographs and pore structure analysis for fully submerged conditions. In these tests, the employed current density levels were higher, i.e. $100\text{mA}/\text{m}^2$ and $1\text{A}/\text{m}^2$. The conditions in these series of experiments can be viewed as mortar in saturated conditions in water and $\text{Ca}(\text{OH})_2$, where in the former case concentration gradient was present, while not relevant for the latter case.

For fully-submerged in water conditions, increased porosity and pore size from 28 days to 112 days were recorded for both $100 \text{mA}/\text{m}^2$ and $1\text{A}/\text{m}^2$ regimes. A more distinct effect of the higher current density, $1\text{A}/\text{m}^2$, was recorded at both 28 days (Fig. 14a) and 112 days (Fig. 14b). For the control specimens, the parallel processes of on-going cement hydration and leaching-out resulted in slightly reduced critical pore size and/or redistribution of the pore network i.e. initially smaller pores became coarser after 28 days due to leaching-out, but similar porosity values were recorded between 28 and 112 days of age, together with reduced critical pore size at 112 days (Fig. 14a, b). The control specimens remained with the lowest porosity throughout the test.

For the specimens, conditioned at the lower current density level regime – $100 \text{mA}/\text{m}^2$, porosity and critical pore size increased, compared to control conditions at 28 days of age (Fig. 14a) and maintained at similar levels for 112 days (Fig. 14b). At both 28 days and 112 days of age, the specimens under $1 \text{A}/\text{m}^2$ current flow presented the highest level of microstructural changes, with increased porosity and critical pore size at the end of the test (Fig. 14a, b). The results from image analysis are well in line with the MIP results (Fig. 6a, b) where

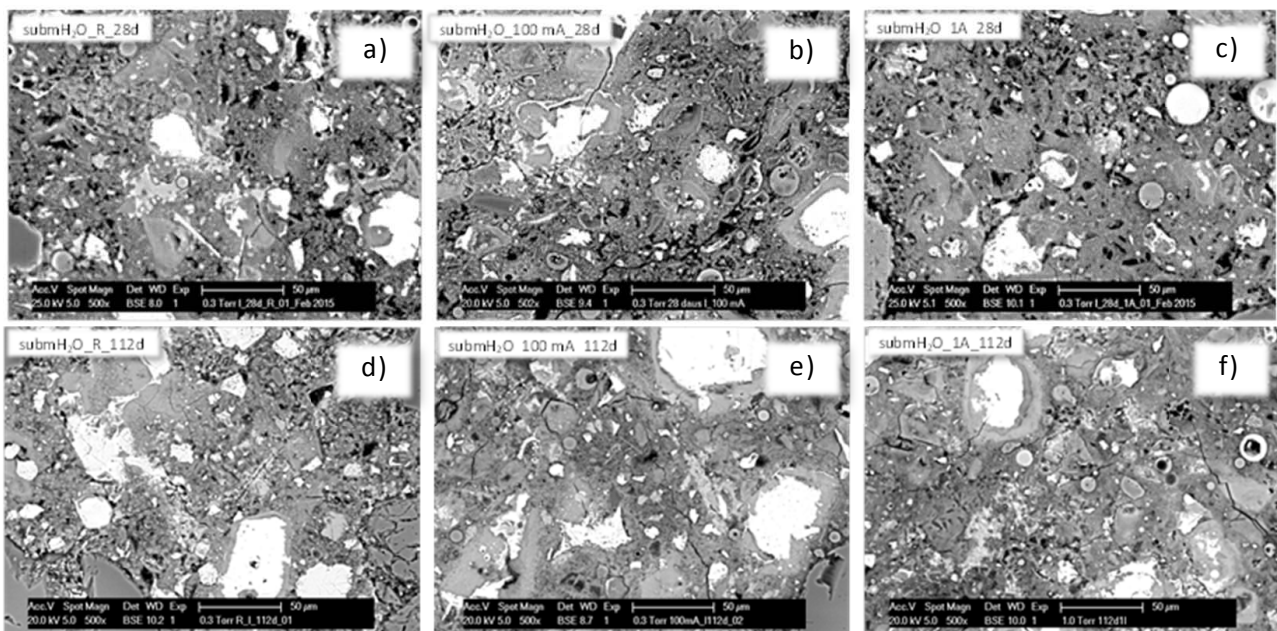


Fig.13 ESEM micrographs 500 \times of mortar bulk matrix at 28 days (top row) and 112 days of age (bottom row) - **fully-submerged in water** conditions for **control** (a, d), “under current” regime of **100 mA/m²** (b,e) and “under current” regime of **1 A/m²** (c, f).

an obvious re-distribution of the pore space was relevant, especially for the “under current” conditions (marked region in **Fig. 6b**). The microstructural investigation (both image analysis and ESEM) are also well in line with the derived compressive strength values (**Fig. 2b**), where a clear trend towards reduction of mechanical properties was recorded with age for the “under current” specimens i.e. at the end of the test, ca. 60 MPa were recorded for control cases, 50 MPa for the 100 mA/m² and 46 MPa for the 1 A/m² regime.

For the *fully submerged in Ca(OH)₂ conditions*, **Figs. 15** and **16**, an entirely opposite trend to the water-conditioned specimens was recorded at 28 days of age (compare **Fig. 15a** and **16a**). The highest porosity and critical pore size were recorded for control specimens, followed by the 100 mA/m² and 1 A/m² regimes (**Fig. 16a**). The trend towards matrix densification maintained at 112 days as well, with no significant difference between the groups of specimens at that age (**Fig. 16b**). This is also visualised by the similar appearance of the bulk matrix in all three conditions at 112 days (**Fig. 15d, e, f**). Mortar specimens, saturated in alkaline medium, would not suffer leaching-out. Hence, the effect of current flow would result in enhanced cement hydration only, consequently in reduced porosity and critical pore size. While this was as observed (**Fig. 16a, b**), image analysis derived similar values for critical pore size at both 28 and 112 days of age for the “under current” regimes, especially the 1 A/m² regime. Observation of the bulk matrix for 1 A/m² conditions at 28 and 112 days also reveals almost no visual morphological changes or appearance (**Fig. 15c, f**).

The MIP results confirm re-structuring of the pore space and family of larger pores (> 0.1 μm, **Fig. 6d**), appearing at 112 days of age for “under current” conditions. These changes were, however, not significant and not responsible for a reduction in mechanical properties, as otherwise observed for the water conditioned test series (**Fig. 2c**). They are an indication, though, for the effect of the higher level of stray current on bulk matrix

properties, even in saturated conditions, where leaching-out is avoided. Consequently, these results need to be taken into account in conditions where higher current densities are involved in practice e.g. above 1 to 5 A/m² as within concrete desalination or re-alkalisation, stray currents, etc. With higher current density, enhanced migration-controlled transport could result in a pore-water dis-balance or internal concentration gradients, leading to undesired changes of the pore structure (e.g. internal leaching, effects similar to self-desiccation, etc.).

The results obtained for Ca(OH)₂ conditioned specimens are in a good agreement with reported experiments (Rafiepour *et al.* 2012), where lower porosity was obtained in lime saturated curing conditions. Additionally, other reports suggest that for specimens submerged in Ca(OH)₂ higher compressive strength is to be expected and recorded, compared to specimens cured in water (Bediako *et al.* 2015, Hayri *et al.* 2011). These dependencies were also observed in this work (**Figs. 5, 6, 14, 16**).

3.4.3 Sealed conditions

Figures 17 to **20** present the microstructural analysis for sealed conditions. These are in fact the most representative ones, as far as the effect of external environment and conditioning are to be split from the effects of stray current only. The employed current densities were at the levels of 100 mA/m² and 1 A/m². The outcomes were compared to equally handled (equally sealed) control cases. The results for sealed conditions refer to two aspects of possible microstructural development and/or changes:

- pore network development in the *bulk matrix only* – referring to the internal, bulk volume of the cubes, as performed for all above discussed test series;
- pore network development of the *matrix in the immediate vicinity of the cast-in metal sheet electrodes*, through which the electrical current was applied for sealed conditions (**Fig. 1c** depicts the locations for sampling of these cubes).

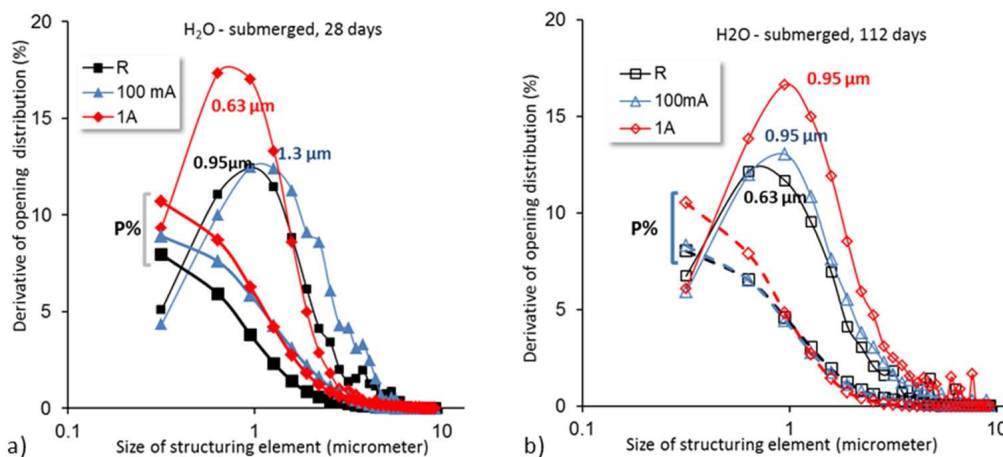


Fig. 14 Porosity and pore size distribution – mortar bulk matrix for control and “under current” regimes of 100mA/m² and 1A/m² in *fully submerged in water* conditions – a) overlay of results for 28 days of age; b) overlay of results for 112 days of age.

3.4.3.1 Bulk matrix in sealed conditions:

Figures 17 and 18 depict results for sealed conditions for the *bulk matrix* (middle section in Fig. 1c). Visual observation revealed similar morphology at both 28 days and 112 days in all conditions (Fig. 17). A slightly coarser structure for the control specimens at 28 days (Fig. 17a, Fig.18) was observed. At each time interval (7, 28 and 112 days), the difference in porosity and pore size between the three investigated cases per hydration age (Fig. 18) was not as significant as was observed for all other, already discussed, test series. In sealed conditions, porosity and critical pore size gradually reduced over time, with both parameters maintaining highest values for the control specimens and lowest values for the 1A/m²-conditioned ones. The results from image analysis also correspond to the outcome from MIP analysis (Fig. 7) and are well in line with the previously

discussed compressive strength results, (Fig. 2d). Consequently, the effect of stray current in sealed conditions can be only considered as a positive one, at least for the duration of this test.

3.4.3.2 Pore network development at interfaces:

Figures 19 and 20 present the results from microstructural analysis in three locations of the sealed mortar cubes for “under current” conditions (see Fig. 1c) i.e. the section close to the positive terminal (anodic), the middle section (bulk) and the section close to the negative terminal (cathodic). The middle section (or bulk matrix) would be comparable as features and pore network parameters to the already discussed “*bulk matrix*” only, depicted in Figs. 17 and 18.

The results and discussion in this section are important in view of practical considerations. In fact, when a

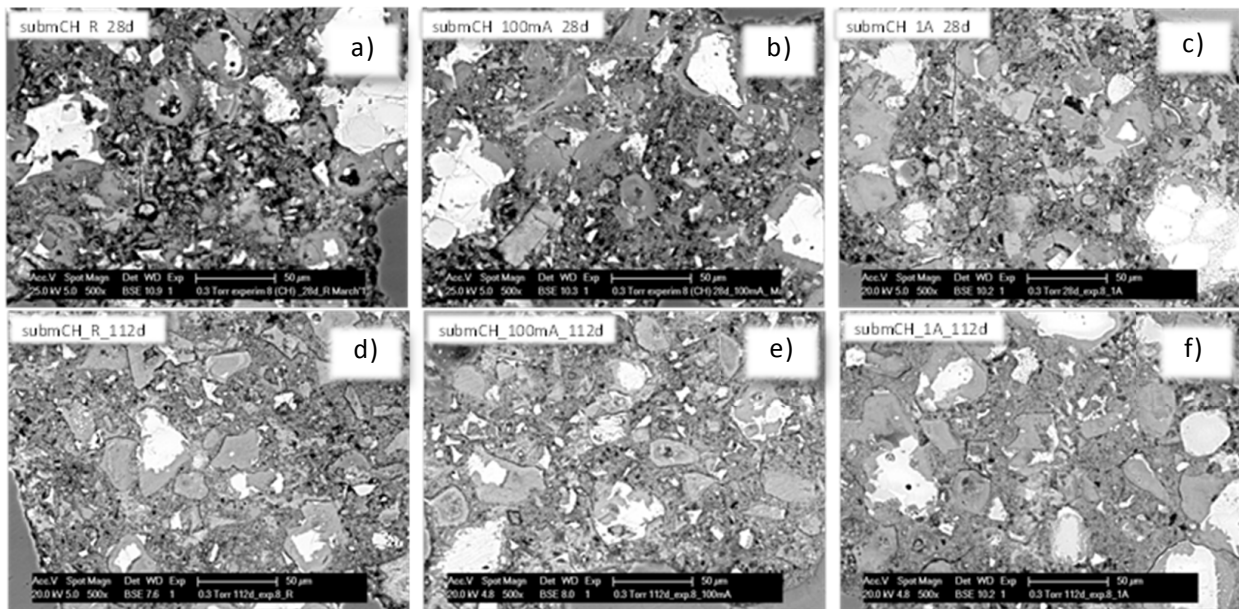


Fig. 15 ESEM micrographs 500x of mortar bulk matrix in *fully- submerged in Ca(OH)₂*: 28 days (top row) and 112 days of age (bottom row) for **control** (a, d), “under current” regime of **100 mA/m²** (b,e) and “under current” regime of **1 A/m²** (c, f).

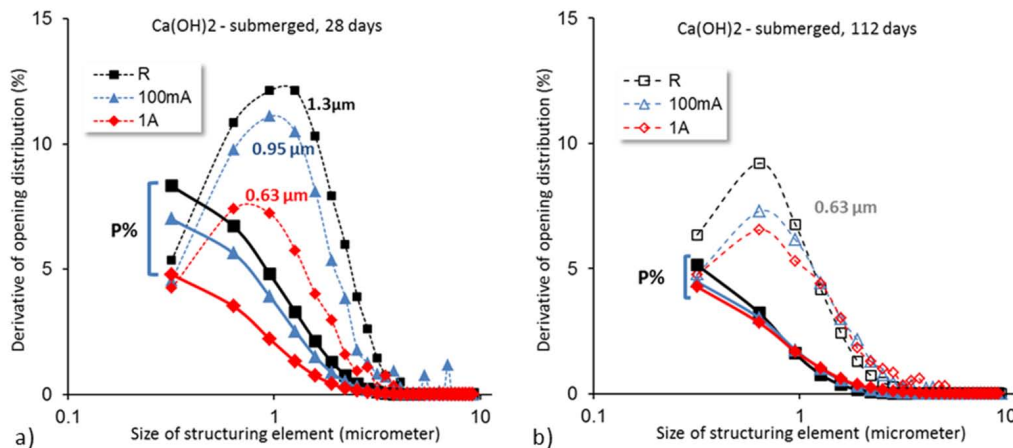


Fig. 16 Porosity and pore size distribution for mortar bulk matrix in control and “under current” regimes of 100 mA/m² and 1 A/m² in *fully submerged in Ca(OH)₂* conditions – a) overlay of results for 28 days of age and b) 112 days of age.

reinforced concrete system is to be evaluated for potential effects of stray currents, the bulk (internal) matrix of the structure is expected to be different in properties from the steel/concrete interfaces. Therefore, microstructural alterations at both areas would determine the overall performance of a structure.

A note here is necessary for the sampling of these cubes: the mortar specimens in this sealed series, can be viewed as a solid electrolyte electrochemical cell. Consequently, a designation of the sides of the cell to anodic and cathodic regions is discussed. When DC current is applied via an external power source, and is flowing through an electrochemical cell, the reactions on the negative terminal will be reduction reactions (this terminal is cathode), while reactions on the positive terminal will be oxidation reactions (this terminal is anode).

Similarly, stray current flowing through a reinforced concrete system results in the development of cathodic (where current flows in) and anodic (where current flows out) locations on the steel reinforcement, potentially affecting differently the cement-based material in the vicinity of these locations. Electrochemical aspects are not subject to this work and will only be discussed to the extent of oxidation/reduction reactions, involving species from the internal pore water, consequently their effect on microstructural changes.

As visualised in Fig. 19, the matrix around the anodic portion of the cubes, (Fig. 19a)), is more similar in appearance and morphology to the bulk matrix, Fig. 19b, e and Fig. 17c, f. In contrast, the matrix at the cathodic portions of the cubes (Fig. 19c, f) appears to be coarser. The pore structure parameters, derived for all locations

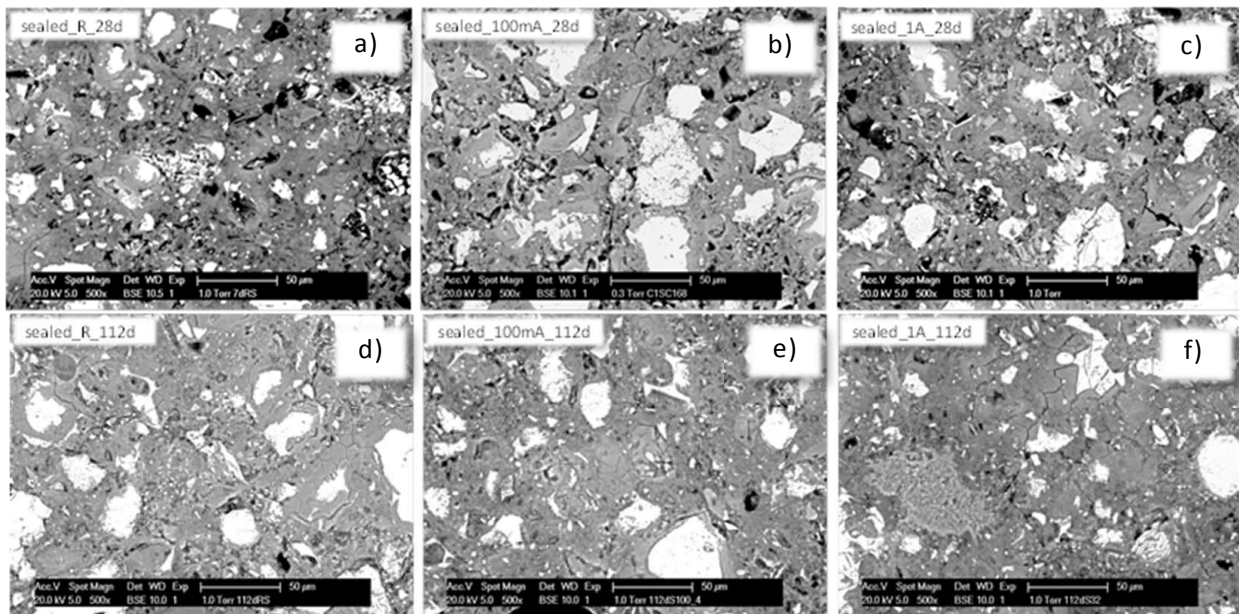


Fig. 17 ESEM micrographs 500x of mortar bulk matrix in **sealed conditions**: 28 days (top row) and 112 days of age (bottom row) for **control** (a, d), “under current” regime of **100 mA/m²** (b,e) and “under current” regime of **1 A/m²** (c, f).

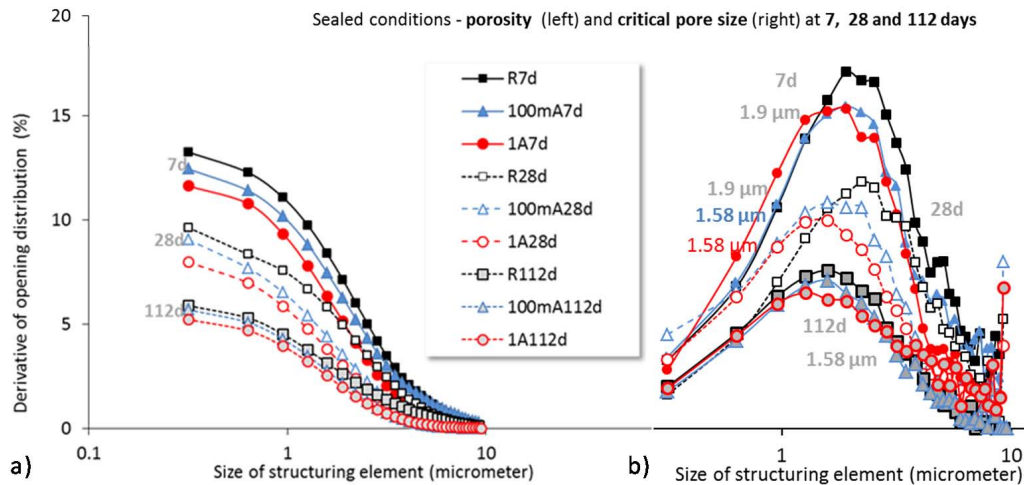


Fig. 18 Porosity (a) and pore size distribution (b) for the bulk matrix of mortar specimens in **control** and “under current” regimes of **100 mA/m²** and **1 A/m²** in **sealed conditions** as an overlay of results for 7 days, 28 days and 112 days.

are summarised in **Fig. 20**, depicting the results for the bulk matrix of the control case (no-current applied) in sealed conditions at 112 days of age (analogical to the already reported specimen R112d in **Fig. 18a, b**). As can be noted, the highest porosity (**Fig. 20a**) and critical pore size (**Fig. 20b**) were recorded for the cathodic regions of the specimens in the 1 A/m^2 regime. Porosity and critical pore size in this region were also higher than the bulk (middle) section regions for the “under current” specimens. In contrast, the derived porosity and pore size for the same (cathodic) location in the 100 mA/m^2 regime, appear to be even slightly lower than those for the middle sections. The lowest porosity and pore size were recorded for the anodic portions of the cubes, with lower values again for the 100 mA/m^2 regime (**Fig. 20a**,

1 A/m^2 anode & 100 mA/m^2 anode; **Fig. 19a,c**).

Obviously, matrix degradation was relevant for the cathodic sides of the cubes i.e. enhanced negative effect on microstructural properties was observed in conditions of 1 A/m^2 current flow. A positive effect was observed at the anodic locations, where densification was relevant for both current regimes. Judging from the very different pore network development between anodic, cathodic and middle sections of the cubes, the 1 A/m^2 regime induced an increase of matrix heterogeneity, reflected by the significant difference in pore network parameters per section of the cubes (**Fig. 20a**). The 100 mA/m^2 regime induced a positive effect, with an obviously more homogeneous distribution of the pore network in the whole cube volume.

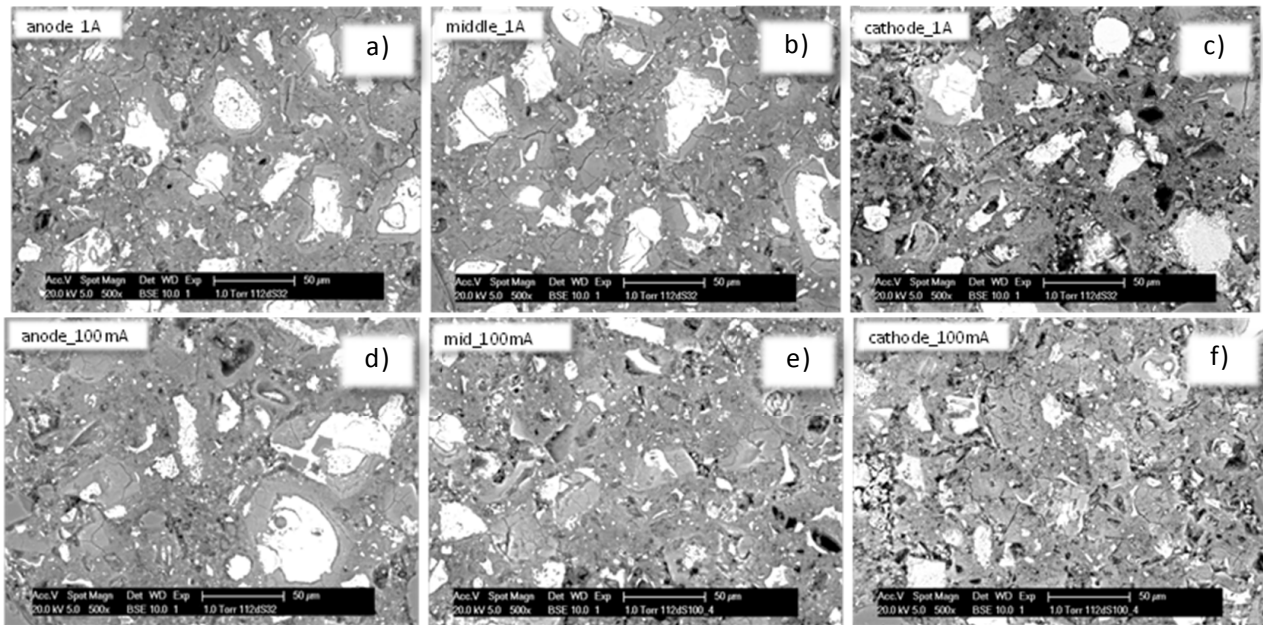


Fig. 19 ESEM micrographs, 500x, of the “anodic” side (left), middle (bulk matrix) (mid) and “cathodic” side (right) (see Fig.1c) of mortar specimens in sealed conditions for “under current” regimes of 1 A/m^2 (top row) and 100 mA/m^2 (bottom row) at 112 days of age.

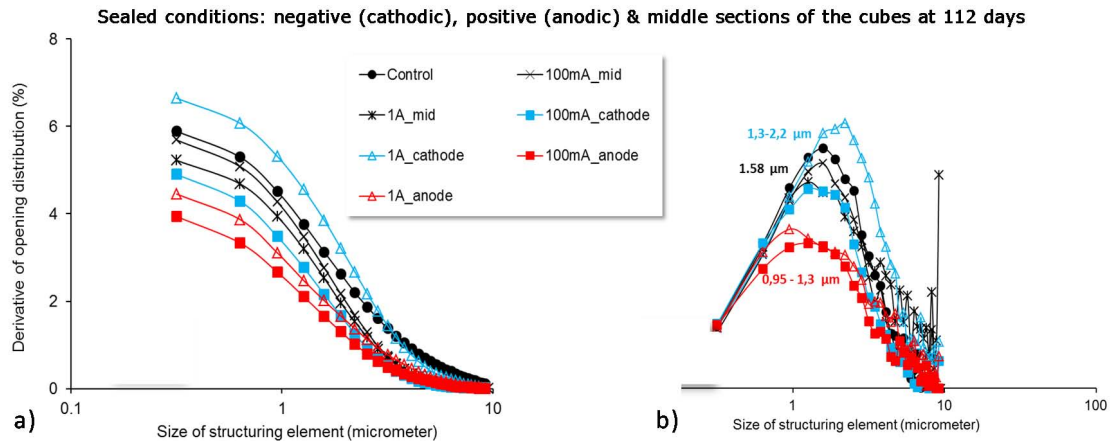


Fig. 20 Porosity (a) and pore size distribution (b) for the bulk matrix of mortar specimens in control and “under current” regimes of 100 mA/m^2 and 1 A/m^2 in sealed conditions as an overlay of results for 7 days, 28 days and 112 days of age.

3.4.3.3 Microstructure in the vicinity of the “anode”

The reactions at the anode (positive terminal) involve oxidation. Among various possibilities (including brass dissolution), anodic reactions involving hydroxyl ions oxidation to water and oxygen were relevant and only considered in this work. The main anodic reaction to be taken into account is the process of oxygen evolution: $4\text{OH}^- \rightarrow \text{O}_2 + 2\text{H}_2\text{O} + 4\text{e}^-$ (or $2\text{H}_2\text{O} \rightarrow \text{O}_2 + 4\text{H}^+ + 4\text{e}^-$, depending on internal equilibrium conditions of H_2O , O_2 and OH^-). In general, pH reduction at anodic locations is possible, following potential availability of H^+ , presence of chloride ions (as within chloride-containing external medium) or CO_2 . In such conditions, and especially at current density levels of more than 100 mA/m^2 , acidification at the anode/cement paste interface would lead to structural deterioration of this interface (Castellote *et al.* 1999). However, for the test series in this work, such conditions in view of external environment, were not present. Consequently, *for the matrix in the vicinity of the anode*, the anodic reaction of oxygen evolution, together with enhanced concentration of OH^- ions (as produced via the cathodic reaction and migrating to the anode), would increase the level of $\text{H}_2\text{O}/\text{OH}^-$ in the vicinity of the anode. The result would be elevated level of pore water, available for the on-going cement hydration and possible densification of the matrix in these locations. This hypothesis for microstructural development in the vicinity of the anode is in fact confirmed by visual observation as well as by pore structure analysis – **Fig. 19** and **20**. Along with the lowest porosity levels (**Fig. 20a**), the lowest critical pore sizes (**Fig. 20b**) were derived for the matrix in the vicinity of the anode.

3.4.3.4 Microstructure in the vicinity of the “cathode”

The reactions at the negative pole (cathode) involve reduction. Similarly, from all possible cathodic processes, those involving water and oxygen reduction were of interest. The main cathodic process for this test series is oxygen reduction: $2\text{H}_2\text{O} + \text{O}_2 + 4\text{e}^- \rightarrow 4\text{OH}^-$. At high current densities, as actually applied in this work, i.e. 100 mA/m^2 and 1 A/m^2 , the region of hydrogen evolution can be reached, therefore the following reaction would be also possible: $2\text{H}_2\text{O} + 2\text{e}^- \rightarrow \text{H}_2 + 2\text{OH}^-$. Both reactions result in an increase of alkalinity (increase of hydroxyl ions) in the vicinity of the cathode. However, only a portion of the hydroxyl ions remains at the cathode and produces a negative ionic charge, while the remaining OH^- migrates to the anode. The excess of negative ionic charge at the cathode is normally counterbalanced by positively charged ions – mainly Na^+ . In other words, at the cathode, the migration of hydroxyl and sodium ions is counterbalanced i.e. accumulation of Na^+ (but also K^+) would be relevant for the cathode, while OH^- migrates to the anode.

The consequence of the above reactions will be en-

hanced alkalinity in the matrix, in addition to the availability of hydrogen gas. The enhanced counterbalance of OH^- with Na^+ , along with H_2 evolution, would account for degradation at the cement paste/cathode interface by simply altering the amount of available OH^- for cement hydration, on one hand. On the other hand, hydrogen gas will occupy empty space at the interface or cause internal pressure in the pore network, leading to coarsening of the matrix (these would potentially be accompanied by elevated heat release as well). The result will be a coarser structure at this interface. Additionally, and as reported elsewhere (Castellote *et al.* 1999), hydration products previously occupying the pore space, would dissolve due to electrical current flow and will result in creating vacancies, hence coarsening of the pore network. This will be in direction of increasing the capillary porosity and especially pronounced at high current density levels (1 to 5 A/m^2) as within desalination or alkalisation, where such side effects would be encountered.

To that end, degradation of the cement-based matrix in the vicinity of the cathode can be expected and was as observed. **Fig. 19c)f** visualises a coarser pore structure at the cathode/mortar interface. **Fig. 20** depicts the results from pore structure analysis, evidencing increased porosity and critical pore size for the matrix in the vicinity of the cathode. Degradation of the matrix in these locations is significant in conditions of 1 A/m^2 , whereas not pronounced at current density level of 100 mA/m^2 , although critical pore size for the latter regime in the “cathodic” part is also higher, compared to the “anodic” and “middle” locations. In fact, what can be observed is that the 100 mA/m^2 current induced comparable alterations at both anodic and cathodic locations.

The above results for the “anodic” and “cathodic” regions and interfaces in sealed conditions are determined by the geometry and experimental set-up. Therefore, no straightforward relations can be made with practical applications, where the proximity or the existence of embedded metallic conductors is not necessarily in similar position. However, the observed behaviour is worth noting and important in view of design and/or within simulations or prognosis for the path and effect of stray currents in practical situations.

3.5 Bulk matrix electrical resistivity

Enhanced ion and water flow (as within electrical current application) would result in altered cement hydration. Leaching-out effects due to diffusion-controlled transport (concentration gradients only) or when both diffusion and migration-controlled transport are present (as within concentration gradients and current flow) will result in mechanical and microstructural changes. All these were observed and discussed in the previous sections. These alterations will in turn affect the development of electrical resistivity in conditions of current flow, if compared to control conditions.

Figure 21 depicts the automatically computed elec-

trical resistivity for mortar specimens per group and per condition. Although more significant variation in electrical resistivity between specimens, conditioned in different regimes might have been expected, such were actually not really observed. More specifically, the results can be viewed as follows:

For partly immersed in water and $\text{Ca}(\text{OH})_2$ conditions (Fig. 21a), resistivity increased with hydration age until approx. 60 days of age and stabilised later-on. The highest values were recorded for the “10mA/m²” regime for $\text{Ca}(\text{OH})_2$ -conditioned specimens, the lowest for the “10 mA/m²” regime of water-conditioned specimens i.e. in both test series the current flow exerted changes in electrical properties. While these were positive in the former case, a negative effect was observed in the latter case – result already commented in view of various aspects in the preceding sections. The results are in line with the recorded compressive strength values (Fig. 2a) and pore structure development (Figs. 7, 8): the lowest compressive strength and highest porosity for the water-conditioned “under current” specimens correspond to the lowest electrical resistivity values for these groups; in contrast, higher compressive strength, lower porosity and highest electrical resistivity correspond to the $\text{Ca}(\text{OH})_2$ -conditioned, “under current” specimens (Fig. 21a).

For the fully submerged in water and $\text{Ca}(\text{OH})_2$ conditions (Fig. 21b, c), the increase in electrical resistivity was more pronounced between 1 day and 60 days of age,

if compared to the partly submerged conditions and, in fact, stabilised earlier – around 35 days of age. This is related to the saturated conditions and altered cement hydration as already previously discussed. The effect of stray current is well seen, although the pattern of resistivity development seems to be similar. The lowest electrical resistivity values for water-conditioned specimens were recorded for the 1A/m² regime, corresponding to the highest derived porosity (Fig. 7a) and lowest compressive strength (Fig. 2b) in these specimens. For the $\text{Ca}(\text{OH})_2$ -conditioned specimens (Fig. 21c), the lowest electrical resistivity corresponds to the control mortar cubes, well in line with their highest bulk matrix porosity (Fig. 7b) and lowest compressive strength (Fig. 2c). The specimens conditioned in $\text{Ca}(\text{OH})_2$ and in 1A/m² regime present the highest electrical resistivity of all saturated specimens (Fig. 9b, c), which is well supported by their highest compressive strength Fig. 2c) and lowest porosity (Fig. 7b).

For sealed conditions a significantly different pattern of electrical resistivity evolution with time was observed (Fig. 21d). Only increasing values were recorded throughout the test, with almost no signs for stabilisation towards the 110 days of age. The results can be interpreted as still on-going cement hydration with time, but this is unlikely to be the effect alone. The most plausible explanation is that in sealed conditions the mortar matrix is insulated from the external environment. Hence water and temperature losses are minimised or

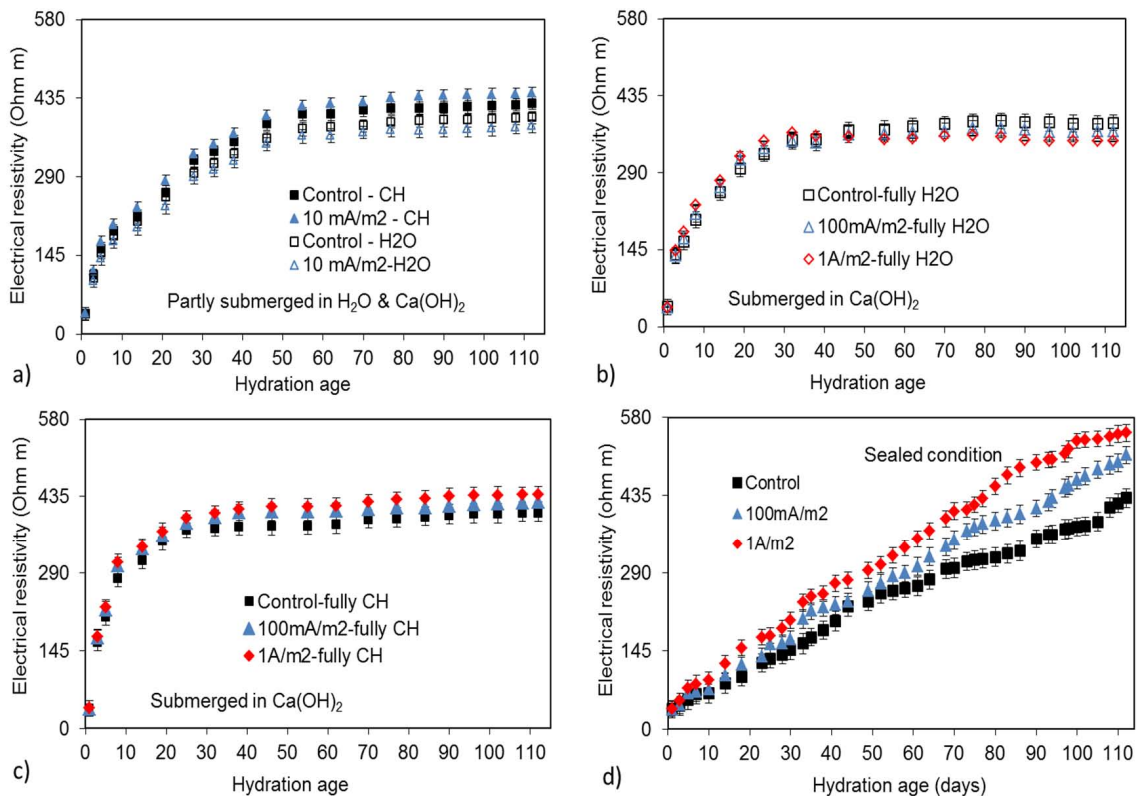


Fig. 21 Evolution of electrical resistivity as a function of hydration age for mortar specimens: (a) partly submerged in water and $\text{Ca}(\text{OH})_2$ solution; (b) fully submerged in water; (c) fully submerged in $\text{Ca}(\text{OH})_2$ and (d) sealed conditions.

none. This, together with the contribution of significantly lower (compared to other test series) relative humidity during measurements, as well as the contribution of the interfacial regions (cast-in terminals and cement paste) in relatively dry conditions, is reflected by a significantly higher values of electrical resistivity, compared to all other cases. Similar to all other groups, the effect of stray current is well seen: the highest resistivity values were recorded for the 1A/m² regime (Fig. 21d), corresponding to highest compressive strength (Fig. 2d) and lowest porosity (Fig. 7c); the lowest resistivity in sealed conditions was recorded for the control specimens (Fig. 21d), completely in line with the lowest compressive strength (Fig. 2d) and highest porosity (Fig. 7c).

Overall, it can be concluded that electrical resistivity is a property of cement-based materials, which indeed reflects well microstructural and transport properties. However, as seen from Fig. 21 it is determined by relative humidity at the most. Therefore, recording electrical properties only, would not be sufficient to derive specific information on pore network development, especially when diffusion- and migration-controlled ion and water transport are both relevant. When such a comprehensive and more specific information would be required, especially in the case of justifying the effect of one or another factor on cement-based material properties (as the hereby evaluated effect of stray current on bulk matrix properties), a combination of techniques, as the hereby employed approach, is necessary.

4. Conclusions

This paper discussed the effect of stray current flow on the development of material properties of mortar in water-submerged, Ca(OH)₂-submerged and sealed conditions. The investigation referred to fresh (24h only cured) mortar, in order to address the practical issue of possible stray current interference within construction work of new buildings and structures. The following conclusions can be drawn:

- Stray current flowing through a cement-based material may cause positive or negative effects on the material properties and performance of the bulk matrix. In general, for fresh cement-based materials, the effect of stray current can be categorized as an effect on early age – e.g. between 1 day and 28 days at the maximum; and an effect on later ages (> 28 days).
- Positive or negative effects of stray current are determined by the external environmental conditions and the level of current density. The former are at hand when concentration gradient with the external medium is avoided or not significant, e.g. for specimens conditioned in alkaline medium or for sealed specimens. Whereas the latter are to be observed in conditions where concentration gradients are present, e.g. water conditioned specimens.
- The contribution of migration-controlled ion and water

transport, as within “under current” conditions, results in enhanced cement hydration at early stages (more significant < 28 days of age). The enhanced cement hydration at early stages results in improved compressive strength and reduced porosity of the matrix. These effects are, however, dependent on the external medium and are only predominant at early age.

- Although a general trend of electrical resistivity increase was recorded over time in all conditions (with on-going cement hydration), the evolution of electrical properties was found to be also dependent on the current density levels and the external medium. For water conditioned specimens, the stray current induced decrease in electrical resistivity if compared to control conditions. For specimens in alkaline medium or sealed conditions, the stray current induced increase in electrical resistivity. The most significant effects (both positive or negative) were observed at the highest current density levels.
- The negative effect of stray current flow on mortar specimens at stages after 28 days of age is mainly attributed to enhanced leaching-out as a consequence of increased ion and water migration when concentration gradients are present. The result was a more pronounced restructuring of the pore space towards coarsening of the pore network (enlargement of initially smaller pores), as otherwise generally known and observed in such circumstances. Water (or neutral to low pH medium) as external environment will be a prerequisite for negative effects, while alkaline medium (or sealed conditions) would minimise or prevent the leaching-out effects.

References

- Alonso, C., Castellote, M., Llorente, I. and Andrade, C., (2006). “Ground water leaching resistance of high and ultrahigh performance concretes in relation to the testing convection regime.” *Cement and Concrete Research*, 36, 1583-1594.
- Aylott, P. J., Cotton, I. and Charalambous, C. A., (2013). “Impact and management of stray current on DC rail systems.” CHAPCIS Intertek, United Kingdom.
- Babaahmadi, A., Tang, L., Abbas, Z., Zack, T. and Martensson, P., (2015). “Development of an electrochemical accelerated ageing method for leaching of calcium from cementitious materials.” *Materials and Structures*, 49(1), 705-718.
- Bediako, M., Kevern, J. T. and Amankwah, E. O., (2015). “Effect of curing environment on the strength properties of cement and cement extenders.” *Materials Sciences and Applications*, 6, 33-39.
- Bertolini, L., Carsana, M. and Pedferri, P., (2007). “Corrosion behaviour of steel in concrete in the presence of stray current.” *Corrosion Science*, 49, 1056-1068.
- Bredenkamp, S., Kruger, D. and Bredenkamp, G. L. (1993). “Direct electric curing of concrete.” *Magazine of Concrete Research*, 45(162), 71-74.

- Carde, C., Francois, R. and Torrenti, J. M., (1996). "Leaching of both calcium hydroxide and C-S-H from cement paste: modeling the mechanical behavior." *Cement and Concrete Research*, 26(8), 1257-1268.
- Castellote, M., Andrade, C. and Alonso, C., (1999). "Changes in concrete pore-size distribution due to electrochemical chloride migration trials." *ACI Mater. Journal*, 96(3), 314-319.
- Charalambous, C. A. and Aylott, P., (2014). "Dynamic stray current evaluations on cut-and-cover sections of DC metro systems." *IEEE Transactions on Vehicular Technology*, 63(8), 3530-3538.
- Chen, Z. G., Qin, C. K., Zhang, Y. J. and Tang, J. X., (2011). "Research of impact of stray current from urban rail transit system on buried gas pipeline." *Advanced Material Research*, Vols. 239-242, 1219-1222.
- Chen, M., Wang, K., Wu, Q. and Qin, Z., (2012). "An experimental corrosion investigation of coupling chloride ions with stray current for reinforce concrete." *Applied Mechanics and Materials*, Vols. 166-169, 1987-1993.
- Cheng, A., Chao, S. J., Lin, W. T. and Chang, J. L., (2012). "Prediction of the deterioration leaching depth of concrete by accelerating calcium leaching test." *Advanced Materials Research*, 365, 3-7.
- Copeland, L. E. and Hayes, J. C., (1953). "The determination of non-evaporable water in hardened portland cement pastes." PCA Bulletin 47, Portland Cement Association, Skokie, IL, USA.
- Copeland, L. E., Kantro, D. L. and Verbeck, G., (1960). "Chemistry of hydration of Portland cement." PCA Bulletin 153, Portland Cement Association, Skokie, IL, USA.
- CUR-Bouw&Infra, (2009). "Duurzaamheid van constructief beton met betrekking tot chloridegeïnitieerde wapeningscorrosie - Leidraad voor het formuleren van prestatie-eisen-." Achtergrondrapport, TU Delft. (in Dutch)
- Diamond, S. and Leeman, M. E. (1995). "Pore size distributions in hardened cement paste by SEM image analysis." *MRS Proc.*, 370, 217-226.
- Faucon, P., Adenot, F., Jacquinet, J. F., Petit, J.C., Cabrillac, R. and Jorda, M. (1998). "Long-term behaviour of cement pastes used for nuclear waste disposal: review of physico-chemical mechanisms of water degradation." *Cement and Concrete Research*, 28, 847-857.
- Faucon, P., Le Bescop, P., Adenot, F., Bonville, P., Jacquinet, J. F., Pineau, F. and Felix, B., (1996). "Leaching of cement: study of the surface layer." *Cement and Concrete Research*, 26, 1707-1715.
- Gaitero, J. J., Campillo, I. and Guerrero, A., (2008). "Reduction of the calcium leaching rate of cement paste by addition of silica nanoparticles." *Cement and Concrete Research*, 38, 1112-1118.
- Galsgaard, F. and Nielsen L. V., (2006). "AC/DC interference corrosion in pipelines." Summary Report by MetriCorr., The Danish Gas Technological Centre.
- Gawin, D., Pesavento, F. and Schrefler, B. A., (2009). "Modeling deterioration of cementitious materials exposed to calcium leaching in non-isothermal conditions." *Comput. Methods. Appl. Mech. Engrg.*, 198, 3051-3083.
- Haga, K., Sutou, S., Hironaga, M., Tanaka, S. and Nagasaki, S., (2005). "Effects of porosity on leaching of Ca from hardened ordinary Portland cement paste." *Cement and Concrete Research*, 35, 1764-1775.
- Hayri, U. N. and Bulent, B., (2011). "The effect of curing temperature and relative humidity on the strength development of Portland cement mortar." *Scientific Research and Essays*, 6(12), 2504-2511.
- Hu, J., (2004). "Porosity of concrete, morphological study of model concrete." Thesis (PhD), Delft University of Technology.
- Hu, J. and Stroeven, P., (2003). "Application of image analysis to assessing critical pore size for permeability prediction of cement paste." *Image Anal. Stereol.*, 22, 97-103.
- Jain, J. and Neithalath, N., (2009). "Analysis of calcium leaching behavior of plain and modified cement pastes in pure water." *Cement & Concrete Composites*, 31, 176-185.
- Kamali, S., Gerard, B. and Moranville, M., (2003). "Modeling the leaching kinetics of cement based materials-influence of materials and environment." *Cement & Concrete Composites*, 25, 451-458.
- Kjellsen, K. O., Monsøy, A., Isachsen, K. and Detwiler, R. J., (2003). "Preparation of flat-polished specimens for SEM-backscattered electron imaging and X-ray microanalysis - importance of epoxy impregnation." *Cement and Concrete Research*, 33(4), 611-616.
- Koleva, D. A., de Wit, J. H. W., van Breugel, K., Veleva, L., van Westing, E. P. M., Copuroglu, O. and Fraaij, A. L. A., (2008). "Correlation of microstructure, electrical properties and electrochemical phenomena in reinforced mortar. Breakdown to multi-phase interface structures." *Materials Characterization*, 59, 801-815.
- Koleva, D. A., (2007). "Corrosion and protection in reinforced concrete: Pulse cathodic protection: an improved cost-effective alternative." Thesis (PhD), Delft University of Technology.
- Kuhl, D., K., Bangert, F. and Meschke, G., (2004). "Coupled chemo-mechanical deterioration of cementitious materials. Part I: Modeling." *International Journal of Solids and Structures*, 41, 15-40.
- Kumara, R. and Bhattacharjee, B., (2004). "Assessment of permeation quality of concrete through mercury intrusion porosimetry." *Cement and Concrete Research*, 34, 321-328.
- Lange, D. A., Jennings, H. M. and Shah, S. P., (1994). "Image analysis techniques for characterization of

- pore structure of cement-based materials." *Cement and Concrete Research*, 24(5), 841-853.
- Laskar, Md. A. I., (1997). "Some aspects of evaluation of concrete through mercury intrusion porosimetry." *Cement and Concrete Research*, 27(1), 93-105.
- Lingvay, C., Cojocar, A., Visan, T. and Lingvay, I., (2011). "Degradation of reinforced concrete structures due to DC and AC stray currents." U.P.B. Sci. Bull., Series B, 73(4), 143-152.
- Maltais, Y., Samson, E. and Marchand, J., (2004). "Predicting the durability of Portland cement systems in aggressive environments—laboratory validation." *Cement and Concrete Research*, 34, 1579-1589.
- Marchand, J. and Bentz, D. P., Samson, E. and Maltais, Y., (2000). "Influence of calcium hydroxide dissolution on the transport properties of hydrated cement systems." In: *Workshop on the role of calcium hydroxide in concrete*; Holmes Beach, Anna Maria Island, Florida, 113-29.
- Marinoni, N., Pavese, A., Voltolini, M. and Merlini, M., (2008). "Long-term leaching test in concretes: An X-ray powder diffraction study." *Cement and Concrete Composites*, 30(8), 700-705.
- Mehta, P. K. and Monteiro, P. J. M., (2001). "*Concrete Microstructure, Properties and Materials*." Englewood Cliffs, NJ USA, Prentice-Hall Inc.
- Nehdi and Soliman, (2011) "Early-age properties of concrete: overview of fundamental concepts and state-of-the-art research." *Construction Materials*, 164, 57-77.
- Neville, A. M., (1981). "*Properties of concrete*." 3rd Ed., London, Pitman.
- Olson, R. A., Neubauer, C. M. and Jennings, H. M., (1997). "Damage to the pore structure of hardened Portland cement paste by mercury intrusion." *Journal of American Ceramic Society*, 80(9), 2454-2458.
- Peelen, W. H. A., Neeft, E. A. C., Leegwater, G., van Kanten-Roos, W. and Courage, W. M. G., (2011). "Monitoring DC stray current interference of steel sheet pile structures in railway environment." *HERON*, 56(3), 107-122.
- Puertas, F., Garcia-Diaz, I., Palacios, M., Gazulla, M. F., Gomez, M. P. and Orduna, M., (2010). "Clinkers and cements obtained from raw mix containing ceramic waste as a raw material. Characterization, hydration and leaching studies." *Cement & Concrete Composites*, 32, 175-186.
- Rafieipour, M. H., Nazari, A., Mohandesi, M. A. and Khalaj, G., (2012). "Improvement incorporating ZrO₂ nanoparticles." *Material Research*, 15(2), 177-184.
- Riskin, J. (2008). "Electrocorrosion and protection of metal: general approach with particular consideration to electrochemical." 1st Ed, Oxford, Elsevier Science.
- Roessler, M. and Odler, I., (1985). "Investigations on the relationship between porosity, structure and strength of hydrated portland cement pastes: 1. Effect of porosity." *Cement and Concrete Research*, 15(2), 320-330.
- Ryu, J-S, Otsuki, N. and Minagawa, H., (2002). "Long-term forecast of Ca leaching from mortar and associated degeneration." *Cement and Concrete Research*, 32, 1539-1544.
- Saito, H. and Nakane, S., (1999). "Comparison between diffusion test and electrochemical acceleration test for leaching degradation of cement hydration products." *ACI Materials Journal*, 96(2), 208-213.
- Saito, H., Nakane, S., Ikari, S. and Fujiwara, A., (1992). "Preliminary experimental study on the deterioration of cementitious materials by an acceleration method." *Nuclear Engineering and Design*, 138, 151-155.
- Scrivener, K. L., (2004). "Backscattered electron imaging of cementitious microstructures: understanding and quantification." *Cement & Concrete Composites*, 26, 935-945.
- Seidell, A. and Linke, W. F., (1953). "*Solubilities of inorganic and metal organic compounds, - A compilation of solubility data from the periodical literature*." New York, Van Nostrand.
- Serra, J., (1982). "*Image analysis and mathematical morphology*." London, Academic Press.
- Struble, L. J. and Stutzman, P. Z., (1989). "Epoxy impregnation of hardened cement for microstructural characterization." *Journal of Materials Science Letters*, 8, 632-634.
- Sumanasooriya, M. S. and Neithalath, N., (2009). "Stereology and morphology-based pore structure descriptors of enhanced porosity (previous) concrete." *ACI Materials Journal*, 106(5), 429-438.
- Sun, Z., Ye, G. and Shah, S. P., (2005). "Microstructure and early-age properties of portland cement paste- Effects of connectivity of solid phases." *ACI Materials Journal*, 102(2), March-April 2005.
- Susanto, A., Koleva, D. A., Copuroglu, O., van Beek, K. and van Breugel, K., (2013). "Mechanical, electrical, and microstructural properties of cement-based materials in condition of stray current flow." *Journal of Advanced Concrete Technology*, 11, 119-134.
- Taylor, H. E. W., (1990). "Cement chemistry." Academic Press, London.
- Ulm, F. J., Torrenti, J. M. and Adenot, F., (1999). "Chemoporoplasticity of calcium leaching in concrete." *J. Eng. Mech. (ASCE)*, 125(10), 1200-1211.
- Wang, Y. Q., Li, W., Yang, X. F., Ye, G., Fan, Q. G. and Zhang, L. P., (2010) "Modeling and simulation the distribution of metro stray current." In: *International Conference on Computer Application and System Modelling (ICCAASM)*.
- Willis, K. L., Abell, A. B. and Lange, D. A., (1998). "Image-based characterization of cement pore structure using Wood's metal intrusion." *Cem. Concr. Res.*, 28 (12), 1695-1706.
- Winslow, D. N. and Diamond, S., (1970). "A mercury porosimetry study of the evolution of porosity in portland cement." *J. Mater.*, 5(3), 564-585.
- Wittmann, F. H., (1997). "Corrosion of cement-based

- materials under the influence of an electric field.” *Mater. Sci. Forum*, 247,107-126.
- Xia, J. and Li, L. Y., (2013). “Numerical simulation of ionic transport in cement paste under the action of externally applied electric field.” *Construction and Building Materials*, 39, 51-59.
- Yang, S. and Yang, X., (2008). “Evaluation of stray current corrosion resistance of concrete in metro construction.” *Front. Archit. Civ. Eng. China*, 2(3), 246-252.
- Ye, G., (2003). “Experimental study and numerical simulation of the development of the microstructure and permeability of cementitious materials.” Thesis (Ph.D.), Delft University of Technology.
- Ye, G., Hu, J., van Breugel, K. and Stroeven, P., (2002). “Characterization of the development of microstructure and porosity of cement-based materials by numerical simulation and ESEM image analysis.” *Materials and Structures*, 35, 603-613.
- Young, J. F., (1988). “A review of the pore structure of cement paste and concrete and its influence on permeability.” *Permeability of Concrete*, 1-18 (ACI SP-108).